

Early and late place cells during postnatal development of the hippocampus

Received: 13 February 2024

Accepted: 6 November 2024

Published online: 21 November 2024

Chenyue Wang^{1,6}, Hongjiang Yang^{2,6}, Shijie Chen¹, Cheng Wang^{2,3,4,5}✉ & Xiaojing Chen¹✉

A proportion of hippocampal CA1 neurons function as place cells from the onset of navigation, which are referred to as early place cells. It is not clear whether this subset of neurons is predisposed to become place cells during early stages, or if all neurons have this potential. Here, we longitudinally imaged the activity of CA1 neurons in developing male rats during navigation with both one-photon and two-photon microscopy. Our results suggested that a largely consistent population of cells functioned as early place cells, demonstrating higher spatial coding abilities across environments and a tendency to form more synchronous cell assemblies. Early place cells were present in both deep and superficial layers of CA1. Cells in the deep layer exhibited greater synchrony than those in the superficial layer during early ages. These results support the theory that an initial cognitive map is primarily shaped by a predetermined set of hippocampal cells.

Spatial navigation and memory are crucial abilities that stem from both innate predispositions and learned experiences^{1–4}. These abilities hinge on the hippocampus^{5–7}, which undergoes a protracted developmental maturation^{8–10}. Various functional cell types in the hippocampus and related regions, such as place cells, grid cells, head direction cells, and boundary/border cells, have been considered as the neural substrates for spatial cognition¹¹. The study of their developmental characteristics has shed light on the mechanisms underlying the maturation of the cognitive map^{12–18}. However, the intricacies of these neural processes involved are not yet fully understood^{2,19}.

Previous studies demonstrated that in early life, a subset of hippocampal neurons functions as place cells^{12,13}, referred to as “early cells”¹², which contribute to the basic cognitive map in early life. An earlier study showed that place cells in rats of postnatal 16 (P16) are capable of remapping in new environments and maintaining stability in familiar ones, indicating the potential for associative memory in

these young animals²⁰. However, it is not known if these early place cells form a distinct class of cells and function as place cells across multiple environments, or if the hippocampus cells form a homogeneous population and cells were randomly recruited to represent a given environment. It is also not clear whether this specific subset of cells serves as the early place cells through early development, or whether other cells have the same chance to become place cells in different days. Additionally, while place cells in infant rats retain their firing location in familiar environments between sessions within hours²⁰, the lifespan of these associative memories is unknown—for example, whether the spatial firing locations can be maintained across days. As the hippocampus matures, the proportion of place cells and the average spatial information (SI) increase^{12–14,21}. However, it remains unclear whether the increased spatial coding ability at the population level stems from an improvement of every individual cell, or, alternatively, from the incorporation of high-capacity cells into the existing

¹Brain Research Centre, Department of Neuroscience, School of Life Sciences, Southern University of Science and Technology, Shenzhen 518055, China.

²Shenzhen Key Laboratory of Precision Diagnosis and Treatment of Depression, Shenzhen-Hong Kong Institute of Brain Science, Shenzhen Institute of Advanced Technology, Chinese Academy of Sciences, Shenzhen 518055, China. ³CAS Key Laboratory of Brain Connectome and Manipulation, the Brain Cognition and Brain Disease Institute, Shenzhen Institute of Advanced Technology, Chinese Academy of Sciences, Shenzhen 518055, China. ⁴Guangdong Provincial Key Laboratory of Brain Connectome and Behavior, the Brain Cognition and Brain Disease Institute, Shenzhen Institute of Advanced Technology, Chinese Academy of Sciences, Shenzhen 518055, China. ⁵Key Laboratory of Brain Cognition and Brain-inspired Intelligence Technology, Chinese Academy of Sciences, Shanghai 200031, China. ⁶These authors contributed equally: Chenyue Wang, Hongjiang Yang. ✉e-mail: cheng.wang1@siat.ac.cn; chenxj@sustech.edu.cn

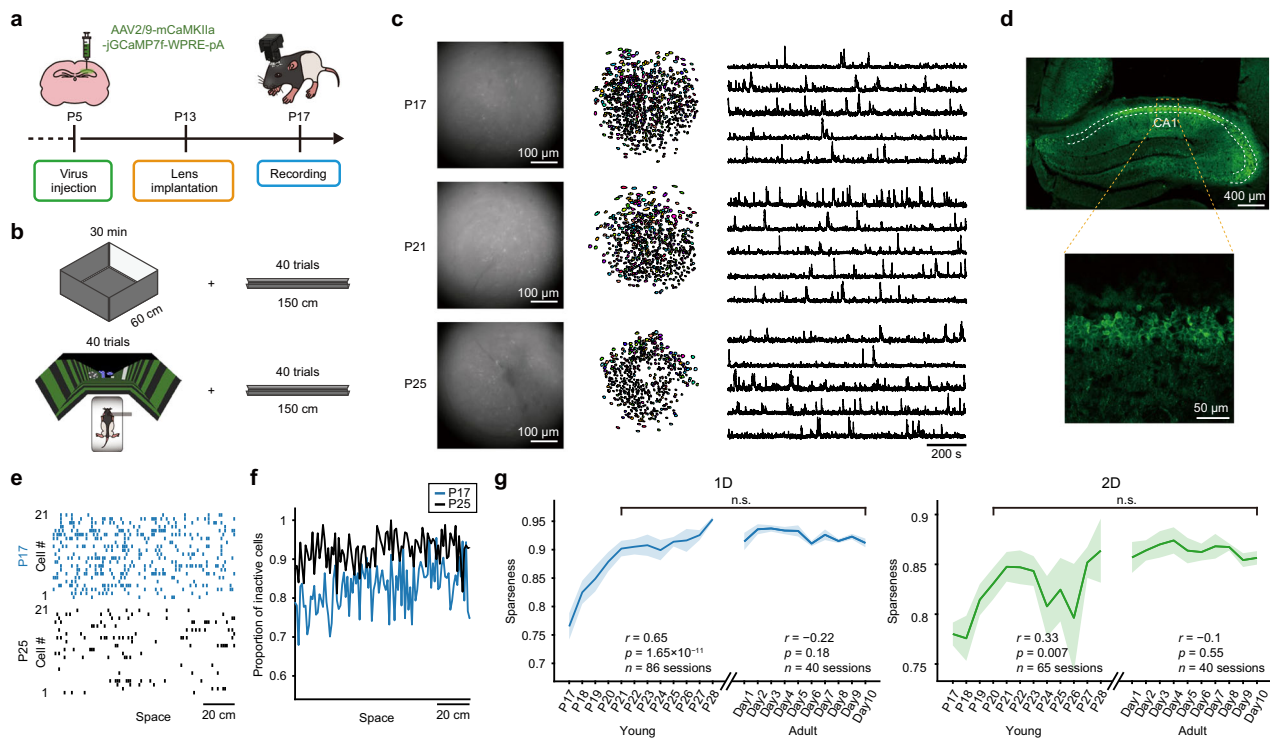


Fig. 1 | Calcium imaging in developing rats performing spatial navigation tasks. **a** Schematics of experimental procedures. **b** Schematics of behavioral protocols. Top: protocol 1, the 2D navigation task and 1D shuttling task; bottom: protocol 2, the head-fixed virtual reality (VR) navigation task and 1D shuttling task. **c** Calcium imaging of hippocampal CA1 at different ages (rows). Left, an example frame from the raw image video; middle, contours of detected neurons; right, representative calcium signal traces from five example neurons. **d** An example of the histological picture showing the expression of GCaMP7f in dorsal hippocampal CA1. **e** Example raster plots of calcium events for cells recorded at postnatal 17 (P17) (top) and P25 (bottom), respectively. **f** The proportion of inactive cells in each spatial bin over an

example spatial segment, representing the population sparseness, corresponding to data in **(e)**. **g** The mean population sparseness across the environment in the 1D shuttling (left) and 2D navigation (right) tasks. The shaded region indicates SEM. For the 1D task, the mean population sparseness increased with age (Pearson correlation coefficient $r = 0.65$, $p = 1.65 \times 10^{-11}$, $n = 86$ sessions), but showed no significant difference from adults starting at P21 (One-way ANOVA: $F_{8, 64} = 1.28$, $p = 0.29$). For the 2D task, the mean population sparseness also increased with age ($r = 0.33$, $p = 0.007$, $n = 65$ sessions) with no significant difference from adults starting at P20 (One-way ANOVA: $F_{9, 54} = 2.02$, $p = 0.062$). Source data are provided as a Source Data file.

network over time¹⁹. Previous studies reported that the coactivation of a neuronal assembly, such as replay and theta sequences, appears and gradually matures from P16 to P24^{21,22}. The relationship between coding abilities and network activity patterns is still unknown.

To address these questions, we adopted the one-photon miniscopy to longitudinally image the population of hippocampal CA1 cells over the developmental process from P17 to P28 while the rats performed multiple spatial tasks. Consistent with earlier studies^{12,13}, we observed a subset of cells that exhibited spatial selectivity during the earliest days, which we referred to as early place cells. In contrast, we defined late place cells as those that initially have low spatial information but develop place fields in later days. Our findings showed that the hippocampal CA1 predominantly used the same group of early place cells to represent multiple environments over the early developmental days, but their place field locations in the same environment altered across early days. With development, the late place cells increased SI more than the early place cells. Moreover, our data revealed that early place cells were inclined to form more synchronous assemblies compared to other cells in early life. Using miniature two-photon microscopy²³, we found that early place cells were present in both deep and superficial layers, with cells in the deep layer displaying greater synchrony than those in the superficial layer.

Results

Increased population sparseness with age

We expressed calcium indicator GCaMP7f in the dorsal hippocampus of neonatal or adult rats and longitudinally imaged the activities of hippocampal CA1 neurons while the animals were performing spatial

tasks (Fig. 1a and Supplementary Fig. 1). A given animal either performed a two-dimensional (2D) foraging task in a square box ($60 \times 60 \text{ cm}^2$) and a one-dimensional (1D) shuttling task on a linear track (150 cm or 100 cm), or, the 1D shuttling task and a virtual reality (VR) navigation task (150 cm) (Fig. 1b and Supplementary Fig. 2). The recording was conducted over a period of 10 to 14 days, either from rat pups aged postnatal day 17 (P17) to P28 or from adult rats aged ~3 months (Fig. 1c, d and Supplementary Table 1, 2).

First, we found that the frequency of the calcium events decreased with development (Supplementary Fig. 3a–f). Then we quantified the sparsity of firing with population sparseness (the percentage of cells that were inactive in that space)²⁴ (Fig. 1e, f and Methods), and observed that the mean population sparseness across the environment increased with age for both 1D and 2D environments (Fig. 1g). From P21 onwards, the population sparseness was not significantly different from that in adults for the 1D environment (Fig. 1g left), whereas no significant difference from adults was observed since P20 for the 2D environment (Fig. 1g right). Notably, in the head-fixed VR environment, the population sparseness was lower than that in the freely moving 1D environment (Supplementary Fig. 3g). The increase in population sparseness with age was consistent across animals (Supplementary Fig. 3h–j).

The increase of spatial selectivity of hippocampal CA1 cells with development

We next investigated the spatial information (SI) content carried by CA1 cells during the developmental process. Same with previous reports^{12,13}, in the 2D environment, spatially informative cells existed at the earliest day tested at P17, with a relatively low number and SI

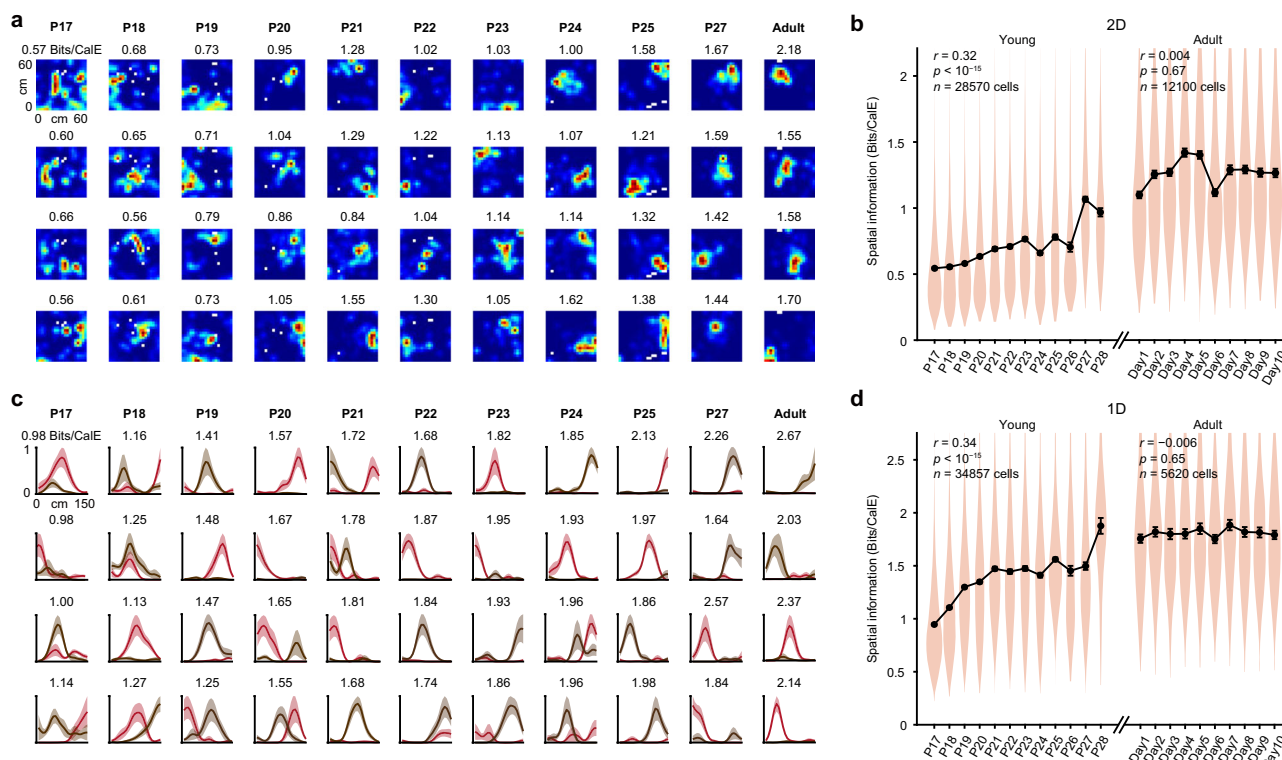


Fig. 2 | The development of spatial coding properties with age. **a** Example spatial rate maps of CA1 cells in the 2D navigation task at various ages. The spatial information (SI) score of each cell was labeled above its rate map. **b** The SI scores of all active cells at different ages in the 2D navigation task. Dots with bars indicate the mean values and the 95% confidence intervals. The SI significantly increased with development (Pearson correlation coefficient $r = 0.32$, $p < 10^{-15}$, $n = 28570$ cells), but showed no changes across recording days in adults ($r = 0.004$, $p = 0.67$, $n = 12100$

cells). **c** Example spatial rate maps of CA1 cells for two running directions (red and brown) in the 1D shuttling task over various postnatal days. The number on top, the mean SI score from the two directions. The shaded region indicates SD. **d** Same as (**b**), but for the 1D shuttling task. The mean SI score for the two directions was used for a given cell. There was a significant increase in SI with development ($r = 0.34$, $p < 10^{-15}$, $n = 34857$ cells), but no changes across recording days in adults ($r = -0.006$, $p = 0.65$, $n = 5620$ cells). Source data are provided as a Source Data file.

(Fig. 2a). The SI scores of all active cells (calcium event number > 20) increased with age (Fig. 2b and Supplementary Fig. 4a). A cell was considered to be a place cell if it met the following criteria: it had a significant SI score ($p < 0.05$), and the SI was larger than that of 35% of all cells (Methods). The proportion and the SI of place cells also increased with development (Supplementary Fig. 4b, c).

For the linear track paradigm, we divided the trajectories into two running directions and calculated the rate maps and SI scores for each direction (Fig. 2c). The SI scores (average SI score for the two directions) of all active cells (calcium event number > 20 in either direction) increased with age (Fig. 2d and Supplementary Fig. 4d). The criteria for a place cell in the linear track were similar to those for the box; additionally, at least 20% of total laps had more than one calcium event (Methods). The proportion and the SI of place cells also increased with development (Supplementary Fig. 4e, f).

Additionally, we examined the spatial representation of CA1 cells in a head-fixed virtual reality (VR) paradigm. Spatial signals could be detected at the earliest day tested in the VR task at P17 (Supplementary Fig. 4g). Consistent with a previous study in adult mice²⁵, the SI was lower in the VR navigation task compared to 1D freely moving task with the same track length (Supplementary Fig. 4h–l). The SI increased with age in the VR task, but at a slower rate compared to 1D freely moving task (Supplementary Fig. 4l). These results suggested that multiple sensory inputs, including vestibular, olfactory, and tactile stimulation, may play a role in the sharpening of spatial representation during early development.

The absolute SI values differed significantly across tasks, possibly reflecting factors including the type of behavioral tasks, the richness of the cues, the dimensions and size of the environments, and the bin size

used for analysis. However, we focused on the developmental change in SI under consistent conditions. Changing the bin size did not affect the ranking of SI values among cell populations in the same environment and did not influence our conclusion that SI increased with age (Supplementary Fig. 4m, n).

Our data showed that the SI reached the adult level around P28 for the 1D task, but not yet for the 2D task. This discrepancy may stem from several factors. First, the linear track task relied more on simple path integration with fixed reset points at the terminals, while the open field task demanded more complex computations without consistent path integration reset points (e.g., by encountering the environmental boundaries). The fixed reset points on the linear track might play a crucial role in error correction, potentially accelerating the development of spatial coding abilities. Second, the restricted path and stereotyped movement on the linear track imposed different cognitive demands than the open field. It is speculated that the 2D task required more complex spatial processing, which might develop more slowly. Furthermore, the size and cue enrichment of each environment might also influence when SI reaches the adult level.

Spatial coding stability across days increased with development

Could place cells maintain consistent spatial firing fields across days in the same environment during early development? We tracked the same cells recorded in adjacent days with a probabilistic method²⁶ (Supplementary Fig. 5a and Methods). For cells classified as place cells in at least one session, we calculated the Pearson correlation coefficients of their spatial rate maps between adjacent days. The place field stability in the 2D environment across consecutive days was low in pre-weaning rats and increased as the animals grew older (Fig. 3a, b and

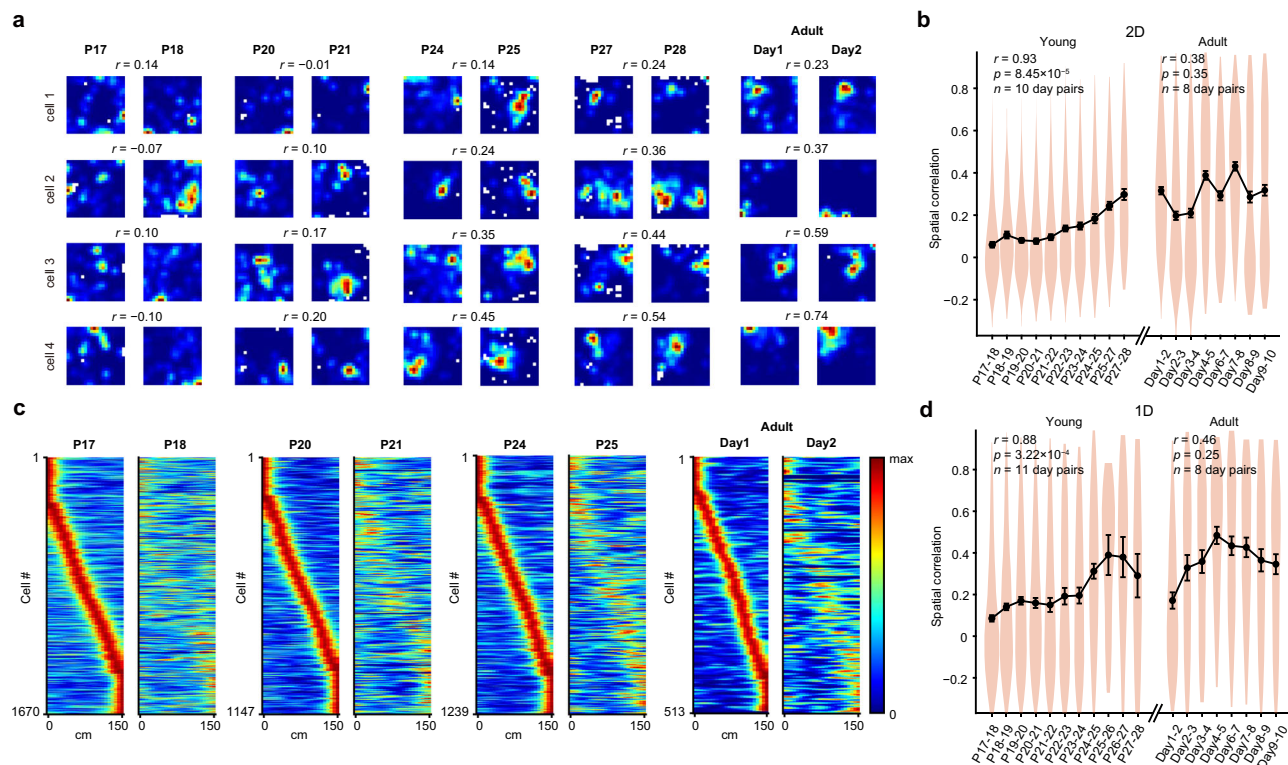


Fig. 3 | The stability of spatial representation of CA1 cells across different ages. **a** Example spatial rate maps for the same cells recorded in the box across adjacent days for different ages. The number on top, the Pearson correlation coefficient of the two spatial rate maps. **b** Correlation of spatial rate maps of the same cells in the 2D navigation task across two consecutive days. Only cells classified as place cells on at least one of those days were included. Data were presented as mean \pm SEM. The correlation of place fields across adjacent days increased with age (Pearson correlation coefficient $r = 0.93$, $p = 8.45 \times 10^{-5}$, $n = 10$ day pairs), but did not

significantly change with the recording days in adults ($r = 0.38$, $p = 0.35$, $n = 8$ day pairs). **c** Sorted spatial rate maps of all cells recorded on the linear track across adjacent days. Only cells classified as place cells in at least one of the sessions (see Methods for criteria) were included. Rate maps for two running directions were treated as independent. **d** Same as (**b**), but for the 1D shuttling task. The correlation of place fields across adjacent days increased with age ($r = 0.88$, $p = 3.22 \times 10^{-4}$, $n = 11$ day pairs), but did not show significant changes with recording days in adults ($r = 0.46$, $p = 0.25$, $n = 8$ day pairs). Source data are provided as a Source Data file.

Supplementary Fig. 5b, c). Similarly, for the 1D environment, the place field stability also increased with age (Fig. 3c, d and Supplementary Fig. 5d–f). Notably, our results showed that the developmental increase in place field stability began at P19–20 in the 2D environment, but from P23–24 in the 1D environment. Similar to the difference of the developmental dynamics of SI between 1D and 2D tasks, the discrepancy in place field stability might also be attributed to the inherent differences in these navigation tasks. The linear track task relied more on sequence encoding within a predictable, repetitive path, whereas the open field task required complex navigation with multiple directions and paths. The development of theta sequences is more pronounced starting from P23 and P24^{21,22}. We speculate that the presence of theta sequences may help stabilize the place fields on the linear track.

The Pearson correlation coefficients (r -values) of spatial rate maps across days vary among different studies using calcium imaging in the rat^{27–29} or mouse hippocampus^{30,31}. These discrepancies might arise from whether place cells are included in both sessions or at least one session, as well as from the criteria used to define place cells. Increased stability holds true when cells in both sessions met the place cell criteria, and these cells showed higher place field correlation compared to cells meeting the criteria in at least one session (Supplementary Fig. 5g). In our study, consistent criteria for identifying place cells were applied to all ages, resulting in a relatively low SI threshold that ensured a representative proportion of place cells in juvenile datasets. Setting the SI threshold higher reduced the proportion of place cells while increasing place field correlation (Supplementary Fig. 5h).

Due to brain growth, cell registration across days was technically challenging in pups compared to adults; however, the spatial correlation was not affected by the registration quality of cell pairs (Supplementary Fig. 5i, j). We also tracked the same cells over several days and observed similar phenomena, that the spatial correlation across early developmental ages was lower than in older ages and adults (Supplementary Fig. 5k–s).

Spatial representation in multiple environments in early developmental stages

Early place cells are defined as those with high spatial coding abilities during initial developmental stages. There was a large dispersion of SI across all CA1 cells in a given environment, with early place cells positioned at the top range. Could the same population of cells be recruited as early place cells across different environments? We analyzed the cells that were active in both 1D and 2D environments, and found that some cells demonstrated above-average spatial selectivity in both environments (Fig. 4a–d and Supplementary Fig. 6a, b). We calculated Spearman's rank correlation of SI values between these two environments for all cells recorded on the same day from P17 to P28 (nine rats), and found a significant correlation between the SI scores from the 1D and 2D environments, specifically in earlier days, and this correlation decreased with age (Fig. 4e, f). These results suggested that, in the early developmental stages, a subset of early place cells exhibited robust spatial coding abilities across environments. As the rats aged, however, most cells displayed mature spatial coding ability. The Spearman's rank correlation of SI scores between environments in adults was comparable to that in P21–22, but lower than in the oldest

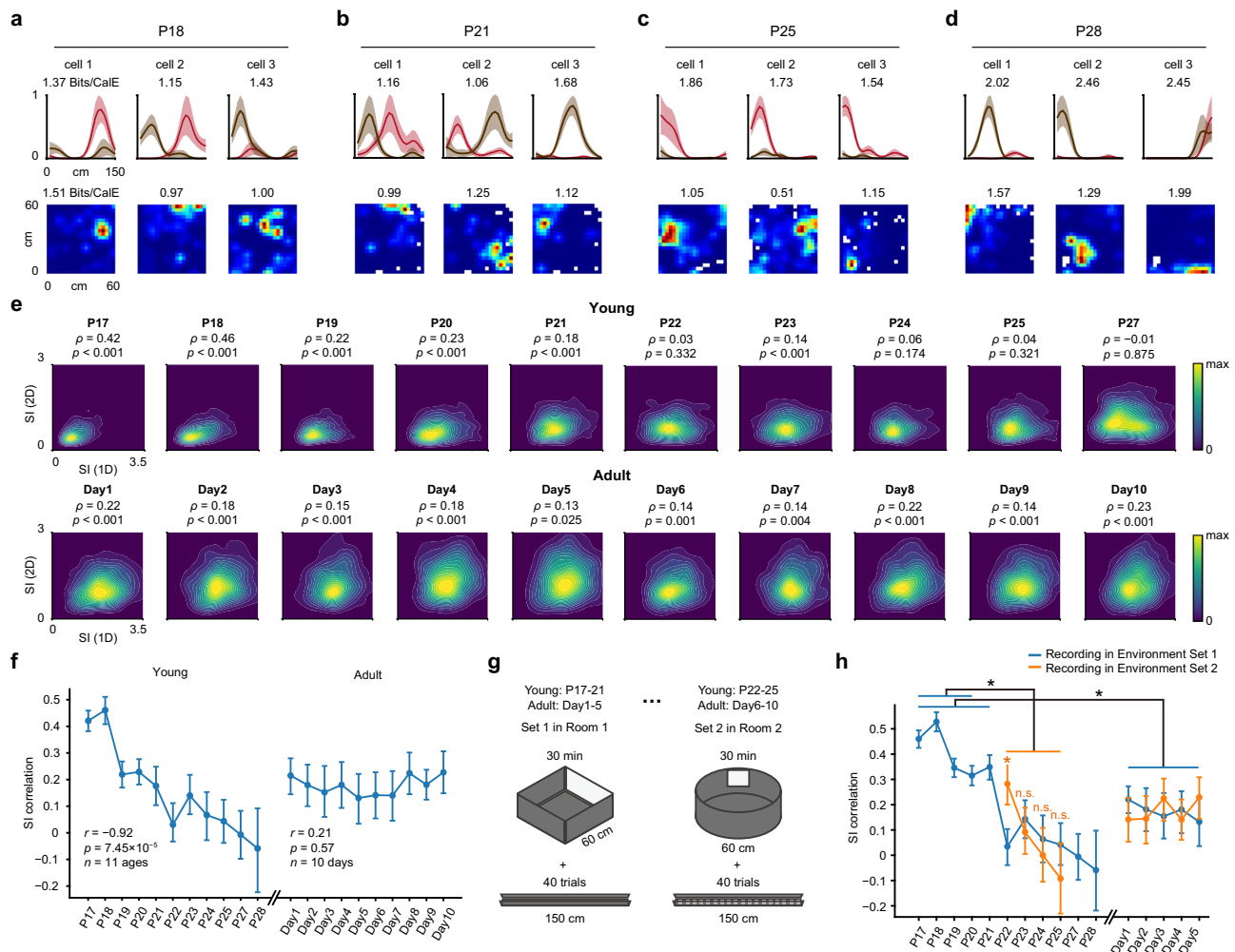


Fig. 4 | Spatial representation for multiple environments during early development. **a** Three example cells (columns) in 1D and 2D environments at P18. Top, rate maps for two running directions on the track; bottom, rate maps in the box. The spatial information (SI) scores were labeled on top. The shaded region indicates SD. **b–d** Same as **(a)**, but for example cells at P21, P25, and P28, respectively. **e** Contour plots showing the distribution of SI scores of the same cells recorded in 1D and 2D environments in developing (top row) and adult (bottom row) rats. The Spearman's rank correlation coefficients of SI scores between two environments and the respective p values were labeled. **f** Spearman's rank correlation coefficients at various ages. Data were presented as observed values \pm the 5th and 95th percentiles of the bootstrapped distribution. The correlation values decreased with age (Pearson correlation coefficient $r = -0.92$, $p = 7.45 \times 10^{-5}$, $n = 11$ ages, 9 rats), but not with the recording days in adults ($r = 0.21$, $p = 0.57$, $n = 10$ days, 5 rats). **g** Schematics

of behavioral paradigms illustrating the employment of a set of novel apparatus in a different room after five days of recording. **h** Comparisons of correlations of SI between 1D and 2D environments under various conditions. Blue: recordings in Environment Set 1 (13 rat pups from P17–21, 9 of which continued for P22–28, and 5 adult rats from Day 1–5). Orange: recordings in Environment Set 2 (4 rat pups from P22–25, which previously exposed to Environment Set 1 from P17–21, and 3 adult rats from Day 6–10). One-sided Permutation tests with Bonferroni correction for the difference of correlation values between groups: P17–20 vs. P22–25 (novel): $p < 0.001$ for each corresponding day; P17–21 vs. Day 1–5 (adults): $p < 0.001$ for each corresponding day; P22–25 (familiar) vs. P22–25 (novel): $p < 0.001$ for P22; $p = 0.20$ for P23; $p = 0.16$ for P24, $p = 0.054$ for P25. Source data are provided as a Source Data file.

pups (Fig. 4e, f). The low correlation in the oldest pups could be attributed to the influence of early-life navigational experiences, whereas in adults, such experiences may have less impact.

To examine whether the observed decrease in correlation with age was a result of increased familiarity with the environments, we introduced an additional four rats to a novel set of 1D and 2D environments from P22 to P25 (novel group), after they had been exposed to previous 1D and 2D environments from P17 to P21 (Fig. 4g). In addition, five adult rats were exposed to the first set of 1D and 2D environments for five days, and three of them also experienced the second set of 1D and 2D environments for an additional five days (Fig. 4g). Results showed that, first, correlation values in the P22–25 novel group were significantly lower than those in the P17–20 group (Fig. 4h). Second, in adult rats, the correlation did not decrease significantly with increased exposure to the environments (Fig. 4h). A

significantly higher correlation values were observed in the P17–21 group than in the adult group (Fig. 4h). Third, from P22–25, there was a significant difference in correlation between the familiar and novel groups at P22, and no significant difference at P23 to P25 (Fig. 4h). Notably, the SI correlation on the first day in Environment set 2 at P22 was significantly higher than that of the sixth day in Environment set 2 at P22, but significantly lower than the first day in Environment set 1 at P17. This result suggested that familiarity affected SI correlation, but not as much as development. Together, these results suggested that the decreased correlation of SI between 1D and 2D environments was more attributed to age than the increased familiarity with these environments.

The Spearman's rank correlation of SI values between 1D and 2D environments based on the rank order of cells' spatial coding abilities within each environment, rather than their absolute SI values. The rank

order of cells' SI within each environment and Spearman's rank correlation between environments were robust to variations in analysis parameters (Supplementary Fig. 6c, d).

Furthermore, we observed that the SI correlation between two running directions on the linear track also decreased with age, but remained constant across recording days in adults (Supplementary Fig. 6e, f). The findings from two directions on the linear track, along with results from two environments (1D and 2D), supported the idea that early place cells were a distinct population that could be recruited for space encoding in multiple environments, although there was no distinct boundary between the spatial coding abilities of early place cells and other cells.

Spatial coding ability of early and late place cells through early developmental stages

Early place cells were those that had high SI and could be categorized as place cells in the initial days by definition. There were two possible scenarios regarding early place cells recruitment each day: first, different populations of cells function as early place cells each day; second, a specific subset of cells is predisposed to be early place cells, maintaining their high spatial coding abilities across days. To explore these possibilities, we monitored the spatial coding ability of the same cells across days.

We observed that the Spearman's rank correlation of SI between adjacent days was higher at early ages in a single environment (Supplementary Fig. 7a–d). Inspired by the observation that, in early developmental stages, cells with high SI in the box also showed high SI in the linear track, indicating robust spatial coding abilities across environments (Fig. 4), we introduced a measure named weighted spatial information (wSI, Fig. 5a and Methods) to quantify the spatial coding ability of a cell across two environments, especially in early-age pups. A high wSI value indicated a high spatial selectivity across environments, and a low wSI indicated a low spatial coding ability in both environments; therefore, early place cells generally had high wSI scores. We found that some cells had high wSI in 1D and 2D environments for two consecutive days (Fig. 5b–d). The wSI between adjacent days was significantly correlated in the early developmental stages, whereas this correlation decreased with age (Fig. 5e, f). For the adults, the wSI correlation between adjacent days was lower than the early developmental ages and remained constant across recording days (Fig. 5f). Furthermore, we examined if the cell's wSI rank changed across days. First, we divided the cells into ten equal groups according to their wSI ranks at each age (Fig. 5g, top). Then, the wSI scores for cells in each group on the subsequent day were calculated, and a linear regression fit was performed for the mean wSI vs. the wSI rank on the prior day (Fig. 5g, bottom). We found that at early ages, the linear fit accurately represented the data, but not at older ages and in adults (Fig. 5g, bottom), which suggested preserved wSI ranks on the subsequent day specifically for earlier ages. The variation in wSI rank over days at older ages could be due to the fact that most cells already had relatively high SI, rendering their specific ranking less pivotal. Moreover, this trend of decreasing wSI correlation with age persisted when rats were exposed to new 1D and 2D environments from P22 (Supplementary Fig. 7e, f). Thus, the high wSI correlation observed in early developmental stages was unlikely to be caused by environmental novelty.

According to studies of Wills et al.¹³ and Langston et al.¹², as well as our data, the percentage and SI of place cells are lower at early developmental ages compared to older ages and adults. Regarding the population-wise increase of SI observed during development, Donato et al. proposed two hypotheses: the first suggests a homogeneous improvement in spatial coding ability across all neurons with age, while the second posits that neurons with high spatial coding ability are sequentially added with development¹⁹. To test this, we compared the developmental time course of the early and late place cells. We

tracked the same cells across the developmental stages over several days, monitoring changes in their SI scores with time (Fig. 5h, i). Because of the rapid growth of the brain and skull during early development, the tracking of cells over several days presented significant challenges; therefore, we limited our tracking to cells in either 1D or 2D environments and only for six days from P17 to P22 to increase the number of cells tracked (Supplementary Fig. 5k). We categorized the cells into six equal groups based on their SI scores at P17. Cells with the lowest initial SI (Group 1) were designated as late place cells, while cells with the initial highest spatial information at initial days (Group 6) were classified as early place cells. We observed that, cells with initially lower SI (late place cells) exhibited a greater increase in SI in the following days, compared to early place cells (Fig. 5h, i). The same analysis conducted on neurons recorded from Day 1 to Day 5 in adults revealed no difference in the dynamics across recording days between the highest and lowest SI groups (Fig. 5h, i).

Further, we identified early place cells as those meeting the place cell criteria at P17, and late place cells as those not meeting the criteria at P17 but meeting them on any day from P18 to P22. The results consistently showed that the SI of late place cells improved more quickly than that of early place cells from P18 and P22 (Supplementary Fig. 7g, h).

These results suggested that the population-level increase in SI with age might be attributed more to the maturation of late place cells, rather than uniform enhancement across all cells. However, we could not determine whether the SI of early place cells slowly increased with development. Firstly, tracking cells across multiple days during development was technically challenging, and we did not obtain enough tracked cells to achieve sufficient statistical power to detect subtle changes of early place cells from P17 to P22. Additionally, we only tracked cells from P17 to P22; a longer tracking period would be needed to observe further changes of early place cells over development, thus we could not ascertain whether high SI place cells in adults originate from early, late, or both types of place cells.

To examine whether newly-emerged late place cells showed the same properties as early place cells at the same age, we analyzed the dynamics of SI for place cells that emerged at various ages with development (Supplementary Fig. 7i, j). Results showed that the SI of P22-place cells was not different from the P17-place cells at P22 (Supplementary Fig. 7k, l). However, due to the small changes in SI of early place cells during development, we could not determine whether the late place cells were more similar to age-matched early place cells or early place cells in the initial days.

The relationship between cell assembly synchrony and spatial coding capability

The increased spatial coding ability of the early place cells may be related to their specific interaction with peer cells within the neural network. We used 1D data to investigate cell assemblies and their synchronization during development, since previous research on the co-activity of hippocampal cells has predominantly utilized data from linear tracks or sleep sessions^{21,32,33}. The population of cells formed distinct cell assemblies, which were characterized by their correlated firing patterns³². We detected cell assemblies from data of the entire session of 1D shuttling task at various ages, using the K-means clustering algorithm (Fig. 6a–g, Supplementary Fig. 8a and Methods). We observed that the number of assemblies detected per session, the number of neurons per assembly, and the number of neurons in the low-correlation clusters decreased with age (Supplementary Fig. 8b–e).

To quantify the degree of synchronization among neurons within an assembly, we employed a measure based on synchronous calcium events (SCEs), named the synchronization index (Fig. 6c and Methods). The synchronization index could be used to assess the signal-to-noise ratio in SCEs vs. other calcium events in an assembly. A higher index

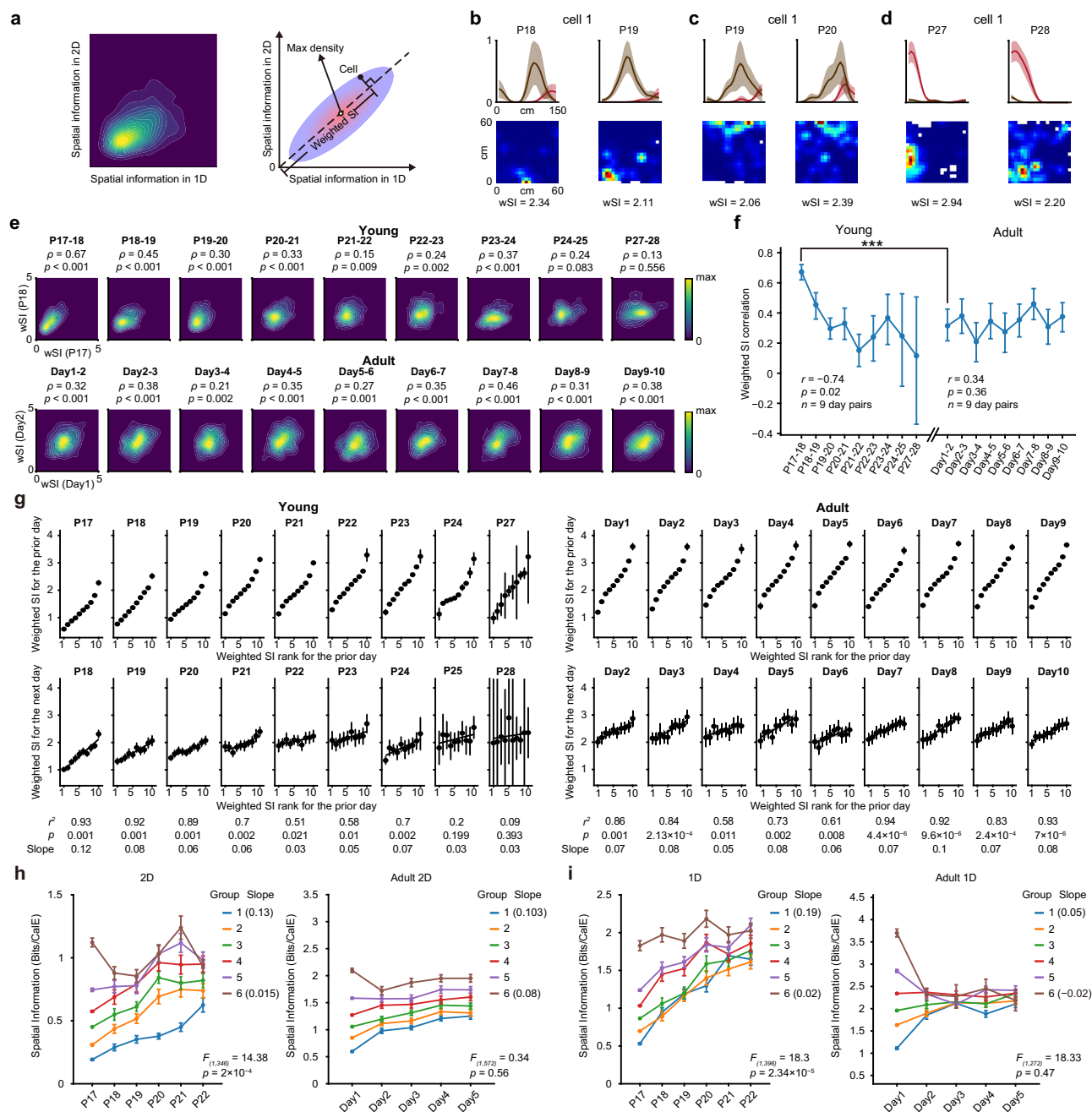


Fig. 5 | Spatial coding ability across days during early development. **a** Left: example contour plot of the distribution of spatial information (SI) in 1D and 2D environments. Right: Schematic for calculating the weighted spatial information (wSI). **b–d** Example cells with high wSI in two consecutive days. Spatial rate maps on the track (top) and in the box (bottom) were shown. The shaded region indicates SD. **e** Contour plots of wSI distribution in adjacent days at various ages. The Spearman's rank correlation coefficients of the wSI between two days and the respective p values were labeled. **f** Correlation of wSI between adjacent days. Data presented as observed values \pm the 5th and 95th percentiles of the bootstrapped distribution. Correlation values decreased with age (Pearson correlation coefficient $r = -0.74$, $p = 0.02$, $n = 9$ day pairs) but not with the recording days in adults ($r = 0.34$, $p = 0.36$, $n = 9$ day pairs). The correlation value at early ages was significantly higher compared to adults (one-sided Permutation test with Bonferroni

correlation, P17-18 vs. Day 1-2: $p < 0.001$). **g** Top: cells divided into ten equal groups based on wSI at each age. Bottom: wSI for the same cells on the following day. Dots with bars indicate mean \pm SEM. A linear regression fit was applied to the mean wSI of ten groups. **h** SI for the cells tracked across many days in the 2D environment. Cells were categorized into six equal groups based on SI at P17 or Day 1 at adult, and linear regression fit was applied to data from P18-P22 or Day 2-5 for each group. Data presented as mean \pm SEM. The slope for Group 1 (lowest SI) was significantly higher than that for Group 6 (highest SI) at early ages (ANCOVA: $F_{1,346} = 14.38$, $p = 2 \times 10^{-4}$), but not for adults ($F_{1,572} = 0.34$, $p = 0.56$). **i** Same as (**h**), but for the 1D environment. Group 1 had a significantly higher slope than Group 6 at early ages (ANCOVA: $F_{1,396} = 18.3$, $p = 2.34 \times 10^{-5}$), but not for adults ($F_{1,272} = 18.33$, $p = 0.47$). Source data are provided as a Source Data file.

reflected a robust signal relative to noise in SCEs, whereas a lower index denoted less distinct SCEs. The synchronization index of an individual neuron was defined as the index of the assembly to which it belonged.

Initially, we examined the sequential activities of the cells around the SCEs in a given cell assembly (Supplementary Fig. 8f–h). We found that in some cell assemblies, the cells exhibited sequential firing (Supplementary Fig. 8i and Methods), which might reflect spatial

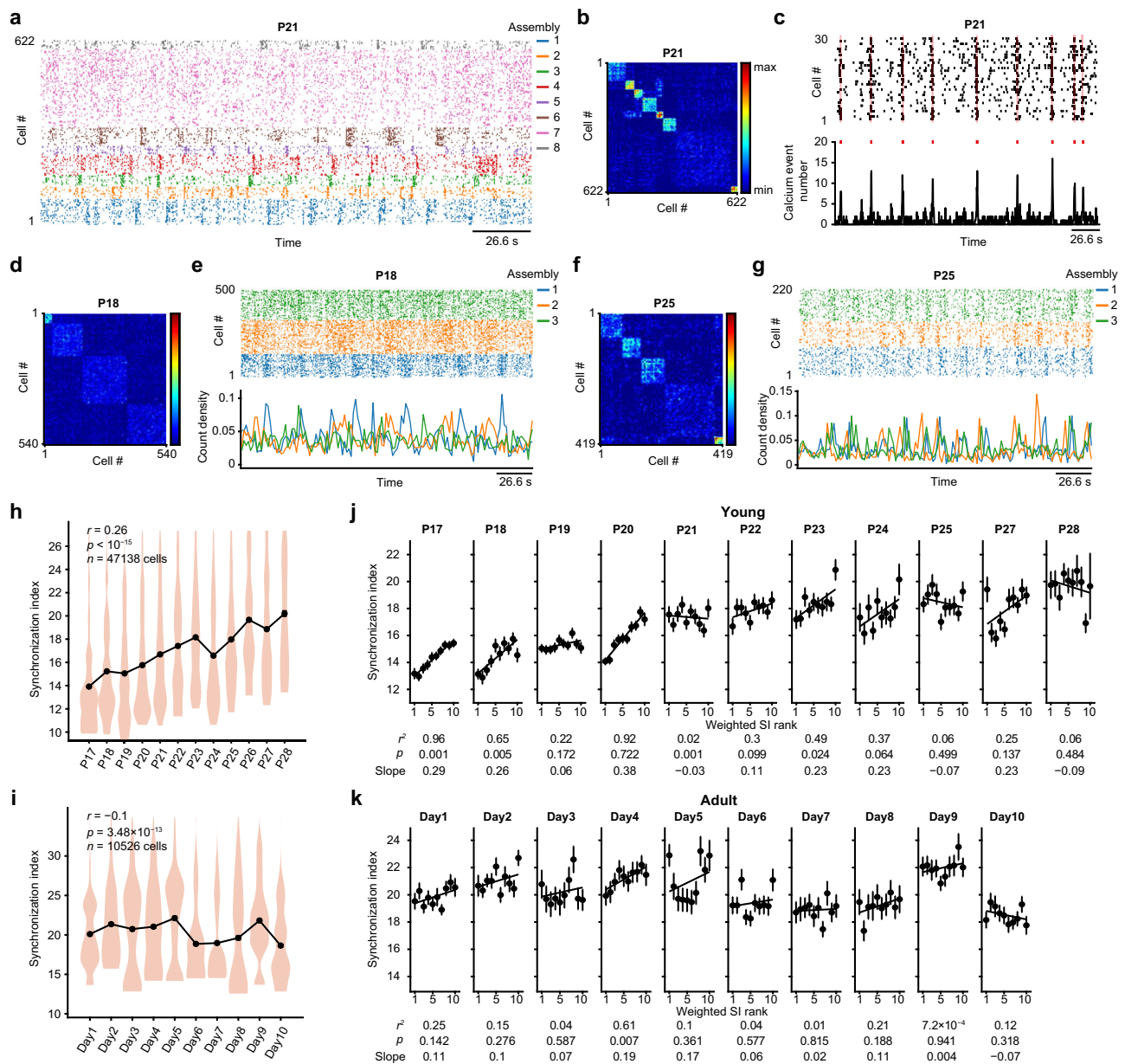


Fig. 6 | Cell assembly properties and spatial coding abilities in early development. **a** An example of raster plots showing cell assemblies detected from all cells recorded in a session on the linear track at P21. These cell assemblies were pre-ordered by a K-means clustering algorithm (see Methods). **b** Correlation matrix of the activities of all cells from the same session as in **(a)**, with cells organized according to the cell assemblies identified in **(a)**. **c** Detection of synchronous calcium events (SCEs) in an assembly. Top, the raster plot of an example assembly recorded at P21; bottom, the histogram of the sum of the calcium events as in top. The shaded red vertical areas at the top and the red bars at the bottom mark the detected SCEs. **d** Correlation matrix for all cells during a linear track session at P18, with cells organized according to the cell assemblies. **e** Top: raster plots of three example cell assemblies from **(d)**. Neurons within the same assembly were labeled

in the same color. Bottom: count density curves illustrating the normalized counts of calcium events in each bin within an assembly. **f, g** Same format as **(d)** and **(e)**, but for a session recorded at P25. **h, i** The synchronization indices for all cells at different developmental ages **(h)** and adults **(i)**. Dots and error bars indicate mean \pm SEM. The indices increased with age (Pearson correlation coefficient $r = 0.26$, $p < 10^{-15}$, $n = 47138$ cells), but not with recording days in adults ($r = -0.1$, $p = 3.48 \times 10^{-13}$, $n = 10526$ cells). **j, k** The relationship between the synchronization index of the cells and their wSI ranks at various developmental ages **(j)** and adults **(k)**. Cells were divided into ten equal groups according to their wSI scores at each age. A linear regression fit was applied across these ten groups. Dots with bars indicate mean \pm SEM. The r^2 values and p values for the fit were labeled at the bottom. Source data are provided as a Source Data file.

coding. However, the proportion of cell assemblies exhibiting this sequential activity was low, only $6.7\% \pm 9\%$ (median \pm IQR) (Supplementary Fig. 8j).

Then we examined the synchrony of cell population during development. Results showed that the synchronization index of all cells increased with age (Fig. 6h), but not with the recording days in adults (Fig. 6i, and Supplementary Fig. 8k). Using weighted SI to represent general spatial coding abilities across environments (Fig. 5a),

we correlated the synchronization index obtained from the 1D task with the wSI derived from both 1D and 2D tasks. The cells recorded each day were divided into ten groups of equal size based on their wSI ranking. The synchronization indices for the cells in each group were calculated for each rank group. A linear regression analysis was performed to assess the relationship between the wSI rank and synchronization index. The results indicated a significant linear correlation between wSI rank and the synchronization index at early

developmental stages, but not in older ages (Fig. 6j). In adults, we did not observe a significant linear correlation between wSI rank and the synchronization index (Fig. 6k). Additionally, we also examined the correlation of the synchronization index and SI in 1D and 2D environments separately (Supplementary Fig. 8l, m). The results consistently showed a high correlation during early developmental stages, but not in older ages or adults. This was in line with our expectations, as early in development, the SI from 1D and 2D tasks were strongly correlated. These conclusions were robust to the method for the detection of the cell assemblies (Supplementary Fig. 8n–r). These findings implied that early place cells were more likely to participate in synchronous network activities.

Both Poisson simulation and rest period analyses suggested that the cell assemblies were unlikely to reflect clustering of place fields (Supplementary Fig. 9 and Supplementary Fig. 10). The SCEs in our data likely reflected a combined effect of theta sequences and replay, which increased with development, consistent with previous studies^{21,22}. Furthermore, the synchronization of cell assemblies might reflect intrinsic connectivity within early place cells.

Developmental properties of cells in deep and superficial layers

Deep and superficial layer cells in the CA1 region have different properties and developmental origins^{34,35}. We thus investigated the distribution and the properties of early place cells in deep and superficial layers. With two-photon imaging, we simultaneously recorded the cells in the deep and superficial cells while young rats were performing the 1D shuttling task and 2D navigation task (Fig. 7a, Supplementary Movie 1, and Supplementary Fig. 11a–j). We recorded 2676 cells in the deep layers and 6073 cells from the superficial layer in 1D and 2D environments (Fig. 7b, c and Supplementary Table 3) from P17 to P19 in three rats. We calculated the basic firing properties of cells in the deep and superficial layers and found no significant difference between them (Supplementary Fig. 11k, l). While previous studies have reported a higher firing rate in deep-layer cells compared to superficial-layer cells in adult rats and mice^{36–38}, our findings in young rats did not reveal such distinctions. It's possible that these differences may develop later in maturation.

We then examined the spatial rate maps in 1D and 2D environments (Supplementary Fig. 12a). Our results showed that the mean SI of cells in the deep and superficial layers was not significantly different in both 1D and 2D environments from P17 to P19 (Supplementary Fig. 12b). Furthermore, we calculated the correlation of the SI between the 1D and 2D environments for cells in different layers at various developmental ages. Results showed that the correlation was higher for the deep-layer cells than for the superficial-layer cells (Fig. 7d, e). The wSI varied with age, but there was no significant difference between the two layers (Fig. 7f). To rule out the possibility that early place cells recorded in our superficial-layer focal plane were actually misidentified deep-layer cells due to hippocampal curvature, we examined the distribution of early place cells in the deep and superficial planes and found no regional clustering. This suggested that the sampling of deep and superficial cells was not affected by the curvature of the hippocampus and did not introduce any artifacts (Supplementary Fig. 12c, d).

To examine the population properties of cells in deep and superficial layers at early developmental ages, we detected the cell assemblies in these two layers respectively (Fig. 7g and Supplementary Fig. 12e). Our data revealed that the deep-layer cells showed a greater synchronization index than the superficial-layer cells (Fig. 7h). Further, we combined the simultaneously recorded cells in deep and superficial layers in a session and detected the cell assemblies. Surprisingly, we found that cells in both layers showed lower synchronization indices than those in the superficial layer only (Fig. 7h). These results suggested that early place cells existed in both layers of CA1. During early

development, cells in the deep layer showed a high SI correlation between different environments and had a higher tendency to form synchronous cell assemblies, whereas cells in the superficial layer showed a slight preference for encoding either 1D or 2D environments and demonstrated lower synchrony.

Discussion

In this study, we longitudinally monitored the calcium activities of a large number of hippocampal CA1 cells from postnatal 17 (P17) to P28. The spatial information content, population sparseness, and place field stability across days all increased with development. In early ages, a consistent population of cells (early place cells) served as place cells across environments and days. Late but not early place cells greatly increased their spatial coding ability. In the initial days, early place cells were more likely to form synchronous assemblies, and present in both deep and superficial layers of CA1. Deep-layer cells were more synchronous and exhibited higher SI correlation between environments compared to superficial-layer cells.

Studies on adult animals showed that place cells maintain stable firing fields over consecutive days in identical environments, both in rats^{39,40} and mice⁴¹. Previous research on young rats revealed that early place cells exhibit lower inter-trial spatial correlation compared to adults^{12,13,20}. Here, our results demonstrated that most early place cells changed their field locations across two days between P17 and P23, with the field stability gradually increasing with age. Behaviorally, an earlier study using a contextual fear conditioning task found that P18 rats exhibited freezing behavior immediately following a shock but not after 24 hours. In contrast, P23 rats were able to recall the shock context 24 hours later⁴². Travaglia et al. employed an inhibitory avoidance paradigm and observed that P17 rats, foot-shocked in one of two compartments, immediately avoided the shocked compartment, but this avoidance behavior did not persist after 24 hours. In contrast, P24 rats avoided the shock compartment 24 hours later⁴³. These behaviors reflect infantile amnesia, and the gradual increase of place field stability we observed might provide a neural substrate for this phenomenon.

In the adult hippocampus, only a small fraction of cells are active in a given environment, reflecting the principle of sparse coding⁴⁴. We found that the development of spatial representation in the hippocampus was accompanied by increased sparseness in neuronal firing. Treves and Rolls demonstrated that the sparseness of the network is essential for the memory capacity⁴⁵. Thus, our finding suggested that the CA1 network was not functionally ready for full-fledged spatial representations in distinct contexts during this period because of the low sparseness. It has been suggested that inhibition is necessary for sparse coding⁴⁶. In the hippocampus, parvalbumin-expressing interneurons mature with age^{47,48}, which might underly the observed increase in population sparseness with development. The progressive maturation of the hippocampal inhibitory circuitry, an augmented neurotransmitter release at CA3-to-CA1 synapses from P15 to P28⁴⁹, the functional development of AMPA receptors in the hippocampus by the end of the third postnatal week⁵⁰, the development of the rules of long-term potentiation^{51,52}, the appearance of grid cells¹³, an increase in the proportion of multi-synaptic boutons from P22 to P100⁵³, and the large number of new granule cells generated in the dentate gyrus in early life, may collectively contribute to the enhanced spatial coding ability observed with development. Dissecting the exact contributions of these factors to the development of spatial coding processes warrants further research.

Our study showed that the developmental increase of spatial coding ability in head-fixed VR task was hindered. This suggested that multiple sensory inputs, including vestibular, olfactory, tactile, proprioceptive signals, and self-posture sensation, which are distinctive in real-world exploration, might play a role in the rapid sharpening of spatial representation during early development. The vestibular,

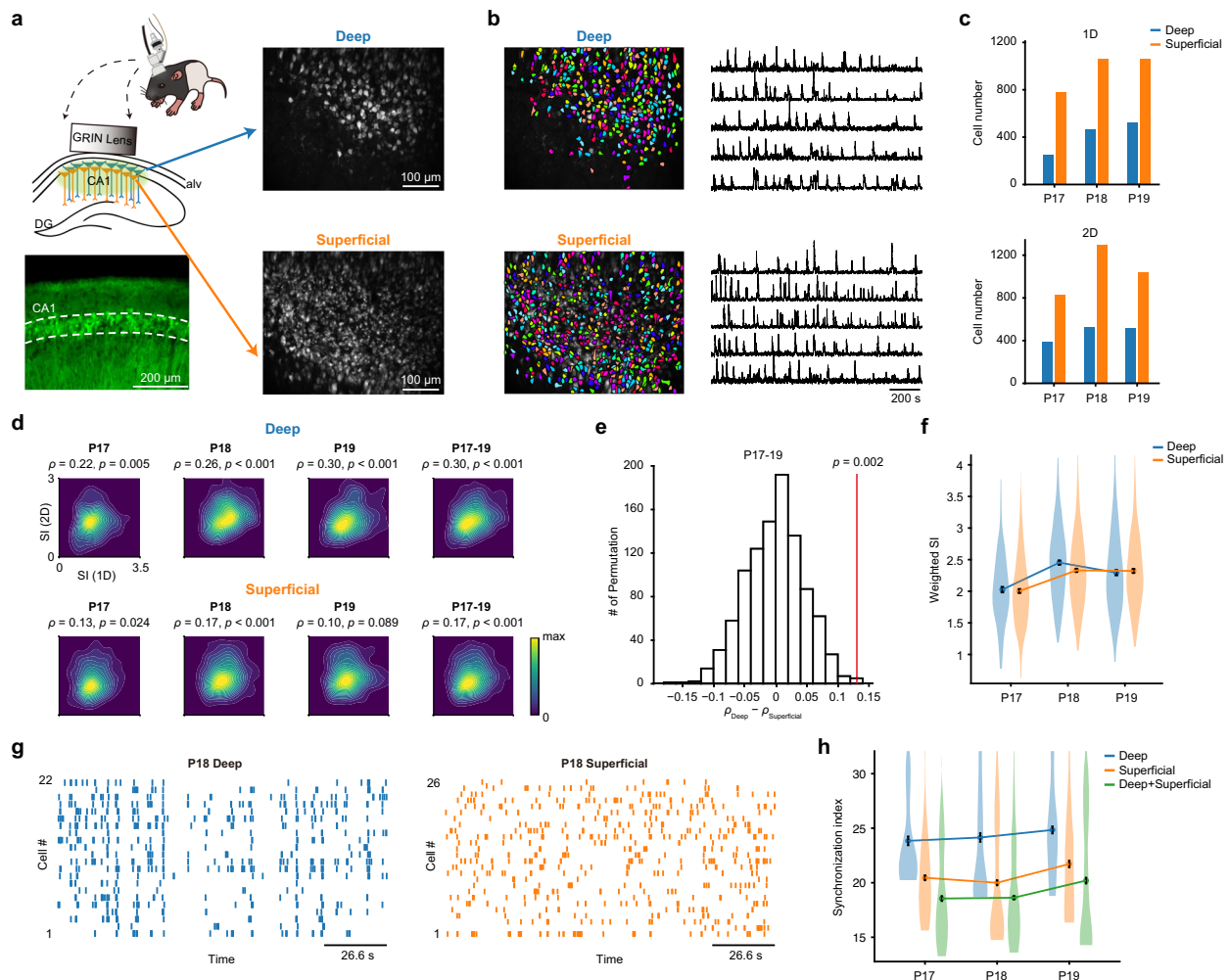


Fig. 7 | The spatial coding and assembly properties of cells in the deep and superficial layers of CA1 during early developmental stages. **a** Top left: the schematic of two-photon imaging, simultaneously recording both deep (blue) and superficial (orange) layers of dorsal CA1 pyramidal cells. Bottom left: an example histological slice showing GCaMP7f expression. Right: the maximum projection images from a recording session, showing the populations in deep (top) and superficial (bottom) layers. **b** Calcium imaging of hippocampal CA1 in deep and superficial layers (rows). Left: Contours of detected neurons. Right: Representative calcium signal traces from five neurons. **c** The number of all cells recorded in deep and superficial layers for 1D (top) and 2D (bottom) sessions. **d** Contour plots of the distributions of the spatial information (SI) in 1D against 2D environments in deep (top row) and superficial (bottom row) layers. The Spearman's rank correlation coefficients of the SI between two environments and the respective p values were labeled. **e** The null distribution of the differences of correlation between the deep

and superficial layers, derived from permuted data. The vertical line indicates the observed difference. One-sided Permutation test: $p = 0.002$. **f** The wSI of cells in two layers at various ages. Data were presented as mean \pm SEM. Two-way ANOVA: age: $F_{2, 1833} = 56.13$, $p < 0.0001$; layer: $F_{1, 1833} = 2.68$, $p = 0.18$; age \times layer: $F_{2, 1833} = 2.68$, $p = 0.69$, 3 rats. **g** Example raster plots showing the calcium events of two cell assemblies in the deep (left) and superficial (right) layers from a session at P18. **h** The synchronization indices for cells in deep (blue), superficial (orange) layers, and for all cells combined (green). Dots with bars indicate mean \pm SEM. Deep vs. superficial layers: Two-way ANOVA: age: $F_{2, 1833} = 8.49$, $p = 2 \times 10^{-4}$; layer: $F_{1, 1833} = 169.74$, $p < 0.0001$; age \times layer: $F_{2, 1833} = 1.53$, $p = 0.21$. Both layers vs. superficial layer: Two-way ANOVA: age: $F_{2, 3015} = 24.23$, $p < 0.0001$; layer: $F_{1, 3015} = 13.99$, $p = 2 \times 10^{-4}$; age \times layer: $F_{2, 3015} = 0.87$, $p = 0.42$, 3 rats. Source data are provided as a Source Data file.

tactile and olfactory systems mature earlier than the visual system and are engaged in exploring the environment at early ages⁹. Head direction cells, whose function depends on the vestibular system, are also the earliest cell type to function in adults^{15,18}. It is possible that early place cells rely on boundary representation and head direction information^{16,54}.

The capabilities for both spatial navigation and learning and memory undergo protracted development⁵⁵, despite key components of the cognitive map, such as head direction cells, place cells, and grid cells, being present early^{12,13} to support basic spatial representation prior to experience⁵⁶. Since navigation is vital for survival in early life, the existence of early place cells before navigational experience may provide “a priori conditions” for spatial cognition⁵⁷. Together with previous works^{3,4,12,13}, our results strongly support the hypothesis that

early spatial coding is contributed by a specific set of early place cells, suggesting an innate neural substrate for initial spatial navigation, while the experience is necessary for the further development of spatial cognition.

In this study, we reported that the early place cells retained their high spatial coding abilities throughout early development. Meanwhile, the late place cells rapidly acquired spatial coding ability with age. It is thus possible that the early place cells provide a genetically preconfigured representation of the environments, aligning with the “nature” aspect of development. It is well known that early experiences are critical for the sculpting of the circuitry and function of the brain⁵⁸. In the hippocampus, the early learning experience is also hypothesized to be critical for the maturation of learning and memory abilities¹⁵⁹. The rapid maturation of the late place cells we observed may be

indicative of their sensitivity and adaptability to early life experiences, environments, or stages of sensory/motor development during early life, reflecting the “nurture” aspect of cognitive development. Thus, the early and late place cell configuration might permit a flexible balance between “nature” and “nurture” for spatial navigation.

Research on human subjects suggested that before the maturation of the hippocampus, particularly the dentate gyrus and CA3, which exhibit more protracted maturation, there is a tendency for the memory system to lean towards generalization in initial learning⁶⁰. In addition, a recent study found that depriving Euclidian geometric experience from birth leads to similar neural representations of different linear tracks³. Our results indicated that the same group of early cells was recruited for the representation of multiple environments, suggesting a contextual generalization in early life. It supported the hypothesis that hippocampal maturation leads to a shift from contextual generalization to specificity, potentially through the development of late place cells.

One mechanism for forming early and late place cells may be of developmental origin. Studies suggest that hippocampal cells sharing the same birthdate exhibit similar connections and functions^{61–63}, making them more likely to form cell assemblies⁶². Consistent with previous findings of coactivation in early place cells^{21,22}, we have found that early place cells were more likely to form coordinated neuronal assemblies compared to the rest of cells during navigation, implying that early place cells could correspond to cells born on the same specific date. On average, deep-layer neurons are born earlier than those in the superficial layer^{61,62,64}. Our two-photon imaging results indicated that early place cells existed in both deep and superficial layers of the CA1. However, due to overlap in anatomical locations of neurons born at different times, whether early and late place cells correspond to cells with distinct birthdates remains an open question. Additionally, we found deep-layer cells demonstrated higher synchronization than superficial-layer ones. The degree of synchronization within each layer exceeded that of combining both layers, suggesting that cells sharing anatomical locations are inclined to synchronize their firing patterns. Moreover, we found the correlation of SI between 1D and 2D environments was higher in deep-layer cells than in superficial-layer cells, indicating that superficial-layer cells have some bias in either environment in early development, supporting the previous finding in adults that superficial-layer neurons excel in differentiating contextual information^{37,65}.

Another potential mechanism for early and late place cells may be distinct gene expression profiles. A recent study showed that neurons in the visual cortex expressing specific biomarkers tend to be more sensitive to visual experiences⁶⁶. It is thus conceivable that early place cells might originate from a genetically distinct cell population. Hippocampal CA1 cells exhibit heterogeneity, and some of them have intrinsic characteristics, such as firing rate, burstiness, etc., suggesting different functional cell types^{67,68}. These functional cell types could potentially correspond to the early and late place cells during the development. For example, early place cells might tend to play a predominant role in spatial representation and might have a higher propensity to become place cells^{68–71}. They may also be the rigid cells that constitute the preexisting neural network⁷². In contrast, the late place cells might correspond to those plastic cells that learn the sequential firing after an experience⁷². This aligns with prior research indicating that hippocampal connections and networks may be at least partly inherently preconfigured^{67,72,73}.

In conclusion, the existence of early and late place cells observed in our study suggested an important functional specialization of the hippocampal cells throughout postnatal development. The dynamic process illustrated the intricate interplay between innate predispositions (“nature”) and learning through experiences (“nurture”), which may confer advantages for initial navigation and adaptation to the surroundings.

Methods

Animals

A total of 32 male Long Evans rats were used in this study, including 27 young rats, and 5 adult rats (about three months old). At postnatal 4 (P4), pups were culled to eight pups per dam to minimize inter-litter variability. Pups were kept with their mother until P21, then they were weaned from their mother and housed in two per cage with the same sex. All animals were housed in a 12-hour light/dark cycle. Behavioral tests and recordings were conducted in the dark cycle. All animal experiments were conducted in accordance with protocols approved by the Animal Care Committee of the Southern University of Science and Technology.

Surgery

The virus carrying the calcium indicator (AAV2/9-mCaMKIIa-jGCaMP7f-WPRE-pA) was injected into the dorsal hippocampus on postnatal day 5 (P5). Rat pups were anesthetized with isoflurane (induction 3%, maintenance 1.5%) and placed on the stereotaxic instrument. The coordinates for virus injection were as follows: 1.8 mm posterior and 1.8 mm lateral to Bregma, 1.9 mm depth from the skull surface. A total of 1000 nl virus suspension (titration at least 1×10^{13} vg/mL) was injected into the right hippocampus within 5 min. The pipette was kept in place for another 5 min after injection to allow sufficient diffusion and prevent backflow. After surgery, pups recovered in a heated chamber (at least 30 min) and were then returned to their mothers.

A 1.8-mm diameter Gradient Refractive Index (GRIN) lens was implanted onto the dorsal hippocampus at P13 or P14. The lens was created by bonding two 1.8-mm diameter GRIN lenses (Edmund Optics, Cat#64519 and Cat#64520) together using optical adhesive (Edmund Optics, Norland Optical Adhesive NOA68). Rats were anesthetized with isoflurane (induction 4%, maintenance 2%) and placed on the stereotaxic instrument. The body temperature was monitored and maintained at 36°C. A craniotomy, measuring 1.8 mm in diameter, was executed, with its center located at 3.4 mm posterior and 2.4 mm lateral to Bregma. Subsequently, the brain tissue above the hippocampus was gently aspirated until the corpus callosum became visible. The corpus callosum was cautiously removed, ensuring the alveus remained intact. Following aspiration, a 1.8 mm GRIN lens was affixed to the stereotaxic instrument and positioned at the center of the craniotomy, then lowered to an approximate depth of 2.1 mm from the skull surface. Initially sealed to the skull with Krazy Glue, the GRIN lens was subsequently secured with dental acrylic. After surgery, animals were administered Dexamethasone and Meloxicam, and were allowed to recover in a heated chamber for 30–50 min, and then returned to their mothers. For the animals that performed virtual reality (VR) navigation task which required head fixation, an aluminum headplate was affixed to the skull, subsequent to the aforementioned procedure.

After a recovery period of two to three days following lens implantation, animals at P16 were anesthetized using isoflurane for evaluation of the expression of jGCaMP7f using a V4 miniscope (<http://miniscope.org>). Upon confirming satisfactory virus expression and calcium imaging quality, the miniscope was adjusted to the optimal focal plane to capture the clearest fluorescence signals. Then, the miniscope's baseplate was affixed to the lens utilizing dental acrylic.

For adult rats, the surgical procedure paralleled that of young rats, albeit with virus injection and lens implantation executed concurrently. In brief, rats were anesthetized using isoflurane (induction at 4%, maintained at 2.5%) and subsequently positioned within a stereotaxic instrument. A 1000 nl virus suspension was injected into the dorsal CA1 (3.8 mm posterior and 2.6 mm lateral to Bregma, 2.8 mm depth from skull surface) over a 5-min period, with the pipette remaining in place for an additional 5 min. Centering around the injection location, a craniotomy of 1.8 mm in diameter was performed, followed by gentle tissue aspiration until the alveus was visibly

exposed. A 1.8 mm GRIN lens was inserted into the craniotomy, approximately 2.7 mm from the skull surface, and was sealed to the skull with Krazy Glue and dental acrylic. After surgery, animals were administered Dexamethasone and Meloxicam. After about three weeks, the baseplate was affixed.

For two-photon imaging, a virus injection was administered to the right dorsal hippocampus at P5, consistent with the procedure for the miniscope imaging. At P13, during the GRIN lens implantation procedure, a baseplate was permanently affixed above the GRIN lens. At P16, the calcium signals were examined using a fast, high-resolution, miniaturized two-photon microscope (FHIRM-TPM V2.0)²³. Briefly, the rat was first head-fixed using the baseplate. Next, a holder for the miniaturized two-photon microscope was attached to the baseplate. Once the imaging areas and focal planes of interest were identified, the holder was permanently secured to the baseplate with dental acrylic.

Histology

Rats were anesthetized using sodium pentobarbital (Sigma, 50 mg/kg, i.p.) and perfused with 0.01 M phosphate buffer solution (PBS, pH7.4), followed by ice-cold 4% paraformaldehyde (PFA) in 0.01 M PBS (pH7.4). Subsequently, the brains were post-fixed overnight in 4% PFA and then transferred to a 30% sucrose solution. The brains were sectioned coronally at 40 μ m using a cryostat, and images were captured using a TissueFAXS Plus S microscope (ZEISS).

Calcium imaging

One-photon miniscope calcium imaging. The calcium signals were recorded utilizing a UCLA open-source V4 miniscope, which was connected to a data acquisition (DAQ) system via a coaxial cable (<http://miniscope.org>). The DAQ system was interfaced with a computer via a SuperSpeed USB 3.0 cable. Calcium images were obtained at a frequency of 30 Hz and a resolution of 608 \times 608 pixels. Behavioral videos were captured at a frame rate of 20 Hz using a webcam, with timestamps provided by the DAQ software to effectively synchronize the calcium and behavioral data.

Two-photon calcium imaging. Calcium signals were captured using a fast, high-resolution, miniaturized two-photon microscope (FHIRM-TPM V2.0) as described by Zong et al.²³. Before recording, the FHIRM-TPM V2.0 was securely fastened to its holder, and rats were allowed a 10-min habituation period. For simultaneous multi-plane imaging, we utilized a removable fast z-scanning module (ZSM) comprising a fast electrically tunable lens (ETL) and a pair of relay lenses. Imaging data of two planes, separated by at least 45 μ m, were simultaneously acquired using the software GINKGO-MTPM (Transcend Vivoscope Biotech Co., Ltd, China) at a frame rate of 9.09 Hz (4.5 Hz cycle rate for each plane, 512 \times 600 pixels) with a femtosecond fiber laser (~35 mW at the objective, TVS-FL-01, Transcend Vivoscope Biotech Co., Ltd, China). The behavior of the rat was monitored with a camera mounted atop the experimental box, illuminated by infrared light. The behavior data was acquired at 25 Hz. The entire system was controlled by custom-developed software GINKGO-MTPM 1.0.2, based on the LabVIEW platform²³.

Behavioral tasks

The 2D navigation and 1D shuttling tasks. Nine juvenile rats engaged in both 2D navigation and 1D shuttling tasks from P17 to P28. Daily recordings were made as the rats freely explored a 2D environment for 30 minutes. After a 10-minute rest period on a pedestal, recordings continued while rats performed 40 trials of running on the linear track. Rat pups did not experience pre-training or food deprivation, and each 1D and 2D environment was novel to them on the initial day of recording. In the 2D navigation task, each rat was placed in the center of a square wooden box (60 \times 60 \times 50 cm³), where it searched for the small, chewable milk tablets. The box, with three black walls and one

white wall, was situated on a disposable kraft paper. In the 1D shuttling task, rats were positioned at one end of a linear acrylic track, either 100 or 150 cm in length with a 5 cm-high edge, and then shuttled back and forth between both ends. The fixed laboratory apparatus provided distal visual cues. At the beginning of the study, we used a 100-cm linear track for three rats (Rat486, Rat529, and Rat542) from P17 to P28. For the remaining rats, we used 150-cm linear tracks.

Four juvenile rats experienced two distinct sets of 1D and 2D environments across two separate periods. From P17 to P21, the rats performed a 2D navigation task within a square wooden box and a 1D shuttling task on a black linear track, both in Room 1. From P22 to P25, they explored different environments in Room 2, performing the 2D task in a circular plastic enclosure (60 cm in diameter) and 1D task on a black-and-white-striped linear track (150 cm long).

Three adult rats also participated in two sets of 1D and 2D tasks: the first set from Day 1 to 5 and the second set from Day 6 to 10. These adult rats were food-restricted to 85% of their body weight and pre-trained in a box on how to forage. Pre-training box was distinct from the ones used during recording sessions. During the first five days, recordings were conducted while the rats performed 2D navigation in the square wooden box and 1D shuttling tasks on the black linear track in room 1. In the following five days, recordings were made in room 2, using the circular plastic enclosure for the 2D task and the black-and-white-striped linear track (150 cm long) for the 1D task.

Two additional adult rats were food-restricted but not pre-trained. These two rats were recorded for five days while performing the 2D navigation within the square wooden box and 1D shuttling on the black linear track in room 1.

For the two-photon imaging experiment, three rats participated in 2D navigation and 1D shuttling tasks from day P17 to P19. Similar to the miniscope imaging procedures, daily recordings included 30 min of free exploration in a 2D environment, followed by a 10-minute rest period without recording, and then 40 trials of back-and-forth running in the 1D environment. The 2D environment was a square acrylic box (60 \times 60 \times 50 cm³), featuring three black walls and one white wall, and was positioned on a white acrylic platform. The 1D environment was an acrylic track of 150 cm and was bordered by a 5 cm-high edge.

For the 1D shuttling task, food reward was applied at the terminals of the track. For the 2D navigation task, food rewards were randomly placed within the box to motivate the animals.

The virtual reality (VR) navigation and 1D shuttling tasks. Three juvenile rats participated in virtual reality (VR) navigation and 1D shuttling tasks from P17 to P28. They were head-fixed onto a treadmill and performed 40 trials in the VR navigation task, followed by a 30-min rest period, and subsequently engaged in 40 trials in the 1D shuttling task.

A 150 cm linear virtual reality (VR) environment was created utilizing a custom setup based on ViRMen⁷⁴. The rat, with the head fixed, ran on a foam treadmill with a 25 cm diameter, and navigated through the virtual environment. The rotation data of the wheel was collected by an optical encoder and relayed to the computer via a micro-controller (Arduino Mega 2560). The VR environment, which displayed two sets of landmarks on each side, was presented on three monitors, each positioned at 108-degree angles relative to each other around the rat. Upon completing the track, underwent a 5-second blackout period, and was then teleported back to the start for the subsequent trial. Behavioral data were synchronized with the calcium signal using a flashing LED, which was visible to a camera and timestamped by DAQ software.

Three additional rats were tested only in 1D shuttling task from P17 to P28.

Immobile sessions. Additionally, five juvenile rats were recorded while they were staying immobile on a small pedestal for approximately 30 minutes each day from P17 to P28.

Data Analyses

Calcium signal processing. For one-photon imaging, calcium signal videos were initially spatially and temporally down-sampled to 304×304 pixels and 7.5 frames per sec, respectively. Then, motion correction was performed using the Non-Rigid Motion Correction (NoRM-Corre) algorithm⁷⁵. The spatial footprint and temporal dynamics of each cell were extracted by the constrained non-negative matrix factorization method for micro-endoscopic data (CNMF-E)⁷⁶. The calcium signals were deconvolved to calcium events, which were estimates of underlying firing rates. The calcium events were used for subsequent analyses.

For two-photon imaging, the open-source software, Suite-2p (<https://www.suite2p.org/>) was used to detect the calcium signals for individual cells⁷⁷. The outputs from Suite-2p were visually supervised using custom MATLAB codes. The fluorescence trace was derived by subtracting the surrounding neuropil signal, computed as follows: $F = F_{\text{measure}} - 0.7 \times F_{\text{neuropil}}$ ⁷⁸. The $\Delta F/F_0$ was calculated as $\frac{F - F_0}{F_0}$, with F_0 determined using a time-averaged median or percentile filter (10th percentile) of F ⁷⁹. The $\Delta F/F_0$ was then deconvolved into calcium events using the fast OOPSI algorithm for further analysis⁸⁰.

A probabilistic approach was employed to register the cells between different sessions²⁶. The distributions of centroid distances and spatial footprint correlations from adjacent cells across multiple recording sessions were modeled to evaluate the probabilities of matching-cell pairs and different-cell pairs. To align cells across four sessions (e.g., 1D, 2D at P17; 1D, 2D at P18), inferences were drawn from cell pairs in the 1D and 2D sessions and sessions on adjacent days.

Behavioral data processing. For one-photon imaging in freely moving rats, the positions of the animals were tracked using a red LED on the Miniscope's CMOS and analyzed offline using custom Python and MATLAB scripts. The behavioral trajectories of the rats were smoothed with a 5-frame boxcar filter (250 ms) and velocity filtered (2.5 cm/sec).

For two-photon imaging in freely moving rats, as there was no LED in the miniaturized miniature two-photon microscope, the animal positions were extracted through DeepLabCut (DLC)⁸¹ (<https://deeplabcut.github.io/DeepLabCut>). The behavior trajectories of the rats were smoothed using the DeepLabCut's default median filter and velocity filtered (2.5 cm/sec).

We also applied the DeepLabCut method to track the locations of three developing rats from P17 to P28 in the one-photon experiment and compared them with the trajectories detected by the traditional LED method.

Rate map and spatial information. Only cells that had enough calcium events (active cells) were included in the analysis. For the 2D navigation and VR navigation tasks, active cells were considered to be cells that had at least 20 calcium events while the animal was running (speed > 2.5 cm/sec) in a session. For the 1D task, cells were considered to be active if they had a minimum of 20 calcium events in either running direction.

For the 2D navigation task, the arena was divided into 3 cm bins, creating a grid of 20×20 . In the case of the 1D shuttling and VR navigation tasks with a 150 cm length, the linear track was segmented into 24 bins (bin size: 6.25 cm). For the 1D shuttling task with a 100 cm length, the track was divided into 4.17 cm sections, also producing 24 bins. Analysis was restricted to bins that had a minimum occupancy of 0.2 seconds. The rate in each bin was calculated by dividing the sum of the calcium event strengths (each weighted by its amplitude) within that bin by the duration of residence in that bin. For the 1D and VR scenarios, the map underwent smoothing with a Gaussian kernel featuring a standard deviation of 2 bins. In the case of 2D, the map was smoothed using a Gaussian kernel with a standard deviation of 1 bin. The spatial information score was calculated by the following

formula⁸²:

$$\text{Spatial information score} = \sum_i P_i \frac{\lambda_i}{\lambda} \log_2 \frac{\lambda_i}{\lambda} \quad (1)$$

In each spatial bin i , P_i is the occupancy probability, λ_i is the activity rate, and λ is the overall mean activity of the cell.

For the 1D shuttling task, rate maps for each of the two running directions were computed separately. The spatial information of a cell was represented by the mean values from the two directions.

To assess the impact of varying bin sizes on spatial information dynamics during development, as well as spatial information correlation between 1D and 2D environments, we standardized the bin size to 3 cm for all behavioral apparatus, resulting in 50 bins for the 150-cm track and 33 bins for the 100-cm track. This standardized bin size was applied only when explicitly stated.

Definition of place cells and spatial correlation across days. For a cell to be considered as a place cell in the 2D navigation task, it had to meet the following criteria: 1) fired more than 20 calcium events post-speed filtering (> 2.5 cm/sec) in the session; 2) the spatial information score exceeded the 35th percentile of all cells; 3) the spatial information score was significantly different from the null distribution. To construct the null distribution, the calcium events of a given cell were circularly shifted by a random amount of time (at least 50 sec) relative to the rat's trajectories, and this procedure was performed 1000 times. The spatial information score was then calculated for each iteration, and the 1000 spatial information scores formed the null distribution. The observed information score was considered to be significant if it was larger than the 95th percentile of the null distribution.

To classify a cell as a place cell in the 1D shuttling task, the neural activity in at least one running direction must meet the following criteria: 1) had more than 20 calcium events after speed filtering (> 2.5 cm/sec) for that specific running direction; 2) the spatial information score exceeded the 35th percentile of all cells; 3) the spatial correlation of odd and even laps was greater than 0.3; 4) at least 20% of total laps had at least one calcium events.

The criteria for identifying place cells in the VR navigation task followed those of a single direction in the 1D shuttling task.

To assess the spatial coding stability in 2D or 1D environments over consecutive days, Pearson correlation coefficients were calculated between the rate maps of two adjacent sessions if the cell was identified as a place cell in at least one of the sessions.

Quantification of data variability using the bootstrap method. A bootstrap method was used to assess the variance of the correlation between spatial information scores in 1D and 2D environments for a group of cells. Specifically, if the group contains n cells, for each iteration, n cells were selected randomly from the pool with replacement, and Spearman's rank correlation coefficient for the bootstrapped cell group was calculated. This process was repeated 1000 times to generate a simulated distribution. Error bars represented the 5th and 95th percentiles from this simulated distribution, illustrating the range of the correlation coefficients.

Permutation test. A perturbation test was performed to assess the difference in the correlation of spatial information scores between 1D and 2D environments for two cell groups. Cells from the two groups, with counts of $n1$ and $n2$, respectively, were combined into a single pool totaling $n1 + n2$ cells. In each iteration, this combined pool was randomly split into two new groups, each with $n1$ for the permuted Group 1 and $n2$ for the permuted Group 2, respectively. Spearman's rank correlation coefficients were then calculated for each of these newly formed groups, and the difference in these coefficients was determined. This process was repeated 1000 times to construct a null

distribution of the differences. The p value was calculated as the proportion of instances in the null distribution where the difference exceeded the observed difference between the original two groups. Bonferroni correlation was applied to the alpha values of the significance level.

The permutation test was also applied to assess the difference in the correlation of weighted spatial information scores between adjacent days.

Weighted spatial information score in 2D and 1D environments. To evaluate the general spatial coding capability across both 1D and 2D environments, we defined a score termed weighted spatial information (wSI) score. This score basically measures the combined information coding abilities across two environments. We adopted this measure as the spatial information scores for the cells in different environments were found to be correlated. Initially, we calculated the spatial information scores of neurons that were active during tasks in both 1D and 2D environments. A scatter plot was created to show the distribution of these scores, with each active neuron represented as a point. We identified the location of max density in this scatter plot using the “*ksdensity*” function in MATLAB. The wSI score of a given cell was then computed as the projected distance onto the line that connects the peak density location and the origin point within the Cartesian coordinate system.

Contour plots. This process involves using scatter plotting and kernel density estimation to analyze 2D scatter data’s spatial distribution. We used the MATLAB function “*ksdensity*” for density estimation on the data points, creating a density estimate for each point. A mesh grid was then created, and the MATLAB function “*interp2*” interpolated these estimates at the original data points. Finally, the MATLAB function “*contour*” was used to visualize the density estimate.

Population sparseness. Population sparseness quantifies the proportion of neurons inactive at a specific spatial location during a session. We only used the rats that performed in the 150-cm track. For both one-dimensional linear track and virtual reality tasks, the track was partitioned into 192 bins, and for two-dimensional open-field arenas, a 50×50 grid was used. For each spatial bin, we defined the population sparseness as the percentage of cells that did not have any calcium event²⁴. The average population sparseness for a session was the mean population sparseness values across all spatial bins.

Cell assembly analyses. Cell assemblies were identified based on their temporal correlations. Initially, calcium events were binned into intervals of 0.266 sec (2 frames). Then, the activity vectors of all neurons were used to construct a correlation matrix. These neurons were then grouped using the K-means clustering algorithm, considering cluster numbers from 5 to 20. To assess the quality of clustering, we utilized the Silhouette index, a metric that gauges the cohesion and separation of clusters. The Silhouette value assigned to each data point indicates its similarity to other points within the same cluster relative to points in different clusters. The optimal clustering configuration was determined by selecting the arrangement with the highest average Silhouette index value⁸³.

To assess the robustness of our results across different cell assembly detection methods, we also applied a hierarchical clustering method⁸⁴. This hierarchical clustering is an unsupervised learning algorithm that partitions data into a tree of clusters. It iteratively merges or splits clusters based on a similarity metric, resulting in a dendrogram that represents the hierarchical relationships among data points. Here, we also set the minimum number of clusters to 5.

Synchronous calcium events (SCEs) and synchronization index. The SCE was a burst of activity by the member neurons of a cell

assembly. SCEs were detected as follows: neuronal activity was first binarized using a 0.266 sec time window; we then calculated the number of calcium events in each temporal bin throughout the session; a particular temporal bin was identified as an SCE if the number of calcium events exceeded a defined threshold ($\text{mean} + 3 \times \text{standard deviation}$).

The synchronization index was used to quantify the degree of synchronization of the SCEs for a cell assembly. The formula for calculating this index is as follows:

$$\text{Synchronization index} = 10 \log \frac{\overline{SCE}}{SC} \quad (2)$$

Here, the numerator \overline{SCE} denoted the average number of calcium events during all SCEs in a given cell assembly, while the denominator SC indicates the average number of calcium events during all activated temporal bins within that assembly. An active temporal bin is defined as one that contains at least one calcium event. A higher synchronization index indicated a high signal-to-noise ratio of the SCEs, whereas a lower synchronization index indicated the opposite.

Sequential activity around the SCEs. For each SCE in a given cell assembly, we defined the baseline firing as the 20% of the peak firing, and thus obtained a time window with the firing above the baseline. For each cell in this assembly, the location of the center of mass (COM) of the calcium events within this window was calculated. The sequence of each cell in this cell assembly was normalized from 0 to 1 based on the COM location of their calcium events in this window. If a cell did not exhibit calcium events within this window, it would have no sequence for this SCE. The session was divided into two halves, each containing an equal number of SCEs. For each half, the average sequence of each cell was calculated by summing the sequences in each SCE window and dividing by the number of SCE windows in which the cell participated. The correlation of average sequences of these cells between the first and second halves of SCEs in a session was calculated, with significant correlation values indicating that these cells exhibited sequential activity.

Poisson firing simulation of cell assembly activity. This section describes the procedure for simulating neural activity using a Poisson process. The spatial rate map determined the instantaneous firing rate for the cell at a particular position in a time bin (note here each calcium event was treated as an action potential, ignoring the amplitude information of the calcium event). To simulate a firing sequence, the inhomogeneous Poisson process was used⁸⁵. A total of 1000 simulations were performed. The simulated neural spikes were analyzed to identify SCEs based on the original cluster’s SCE thresholds.

Statistics

All statistical analyses were performed using MATLAB (MathWorks). To evaluate significant changes in parameters with age in pups or with recording days in adults, Pearson correlation coefficients were calculated between the parameters and ages. One-way ANOVA tests were conducted to determine significant differences in mean population sparseness among multiple groups. Permutation tests were employed to assess the difference in the correlation of spatial information scores between 1D and 2D environments, as well as the difference in the correlation of weighted spatial information scores between adjacent days. ANCOVA tests were used to compare the difference in the slopes of spatial information dynamics with development. A p -value of less than 0.05 was considered significant, and Bonferroni correction was applied for multiple comparisons between groups.

The spatial tuning curves on the linear track for each cell were presented as mean \pm standard deviation (SD). Differences in behavioral trajectories between red LED tracking and DeepLabCut, as well as the

frames of windows for detecting sequential activities in cell assemblies, were presented as the median and interquartile ranges (IQRs). Spatial information scores for each age were presented as mean values with 95% confidence intervals. The variation of the correlation of spatial information scores between 1D and 2D environments, as well as the correlation of weighted spatial information or spatial information between adjacent days, were presented by the 5th and 95th percentiles of the bootstrapped distribution. All other data were presented as standard error of the mean (SEM).

Reporting summary

Further information on research design is available in the Nature Portfolio Reporting Summary linked to this article.

Data availability

Source data are provided with this paper. All data necessary to interpret, verify, and extend the research in this study have been deposited on GitHub under the accession code: <https://github.com/XiaojingChenLab/EarlyPlaceCell>. Due to the large file size, the original calcium imaging videos are available upon request. Source data are provided with this paper.

Code availability

The custom codes specific to this study, along with the data, can be accessed under the following links: <https://github.com/XiaojingChenLab/EarlyPlaceCell> and <https://doi.org/10.5281/zenodo.13911919>⁸⁶.

References

- Bessières, B., Travaglia, A., Mowery, T. M., Zhang, X. & Alberini, C. M. Early life experiences selectively mature learning and memory abilities. *Nat. Commun.* **11**, 628 (2020).
- Donato, F. et al. The Ontogeny of Hippocampus-Dependent Memories. *J. Neurosci.* **41**, 920–926 (2021).
- Farooq, U. & Dragoi, G. Experience of Euclidean geometry sculpts the development and dynamics of rodent hippocampal sequential cell assemblies. *Nat. Commun.* **15**, 8417 (2024).
- Ulsaker-Janke, I., Waaga, T., Waaga, T., Moser, E. I. & Moser, M.-B. Grid cells in rats deprived of geometric experience during development. *Proc. Natl Acad. Sci.* **120**, e2310820120 (2023).
- Scoville, W. B. & Milner, B. Loss of recent memory after bilateral hippocampal lesions. *J. Neurol. Neurosurg. Psychiatry* **20**, 11–21 (1957).
- O'Keefe, J. & Nadel, L. The hippocampus as a cognitive map. *Behav. Brain Sci.* **2**, 487–494 (1979).
- Morris, R. G., Garrud, P., Rawlins, J. N. & O'Keefe, J. Place navigation impaired in rats with hippocampal lesions. *Nature* **297**, 681–683 (1982).
- Bachevalier, J. & Beauregard, M. Maturation of medial temporal lobe memory functions in rodents, monkeys, and humans. *Hippocampus* **3**, 191–201 (1993).
- Wills, T. J., Muessig, L. & Cacucci, F. The development of spatial behaviour and the hippocampal neural representation of space. *Philos. Trans. R. Soc. Lond. B Biol. Sci.* **369**, 20130409 (2014).
- Tan, H. M., Wills, T. J. & Cacucci, F. The development of spatial and memory circuits in the rat. *Wiley Interdiscip Rev Cogn Sci* **8**, (2017).
- Moser, E. I., Moser, M.-B. & McNaughton, B. L. Spatial representation in the hippocampal formation: a history. *Nat. Neurosci.* **20**, 1448–1464 (2017).
- Langston, R. F. et al. Development of the Spatial Representation System in the Rat. *Science* **328**, 1576–1580 (2010).
- Wills, T. J., Cacucci, F., Burgess, N. & O'Keefe, J. Development of the Hippocampal Cognitive Map in Prewanling Rats. *Science* **328**, 1573–1576 (2010).
- Scott, R. C., Richard, G. R., Holmes, G. L. & Lenck-Santini, P.-P. Maturation dynamics of hippocampal place cells in immature rats. *Hippocampus* **21**, 347–353 (2011).
- Tan, H. M., Bassett, J. P., O'Keefe, J., Cacucci, F. & Wills, T. J. The development of the head direction system before eye opening in the rat. *Curr. Biol.* **25**, 479–483 (2015).
- Bjerknes, T. L., Moser, E. I. & Moser, M.-B. Representation of Geometric Borders in the Developing Rat. *Neuron* **82**, 71–78 (2014).
- Muessig, L. et al. Environment geometry alters subiculum boundary vector cell receptive fields in adulthood and early development. *Nat. Commun.* **15**, 982 (2024).
- Bjerknes, T. L., Langston, R. F., Krüge, I. U., Moser, E. I. & Moser, M.-B. Coherence among head direction cells before eye opening in rat pups. *Curr. Biol.* **25**, 103–108 (2015).
- Donato, F., Xu Schwartzlose, A. & Viana Mendes, R. A. How Do You Build a Cognitive Map? The Development of Circuits and Computations for the Representation of Space in the Brain. *Annu. Rev. Neurosci.* **46**, 281–299 (2023).
- Muessig, L., Hauser, J., Wills, T. J. & Cacucci, F. Place Cell Networks in Pre-weanling Rats Show Associative Memory Properties from the Onset of Exploratory Behavior. *Cereb. Cortex* **26**, 3627–3636 (2016).
- Farooq, U. & Dragoi, G. Emergence of preconfigured and plastic time-compressed sequences in early postnatal development. *Science* **363**, 168–173 (2019).
- Muessig, L., Lasek, M., Varsavsky, I., Cacucci, F. & Wills, T. J. Coordinated Emergence of Hippocampal Replay and Theta Sequences during Post-natal Development. *Curr. Biol.* **29**, 834–840.e4 (2019).
- Zong, W. et al. Miniature two-photon microscopy for enlarged field-of-view, multi-plane and long-term brain imaging. *Nat. Methods* **18**, 46–49 (2021).
- Kammerer, A. & Leibold, C. Hippocampal remapping is constrained by sparseness rather than capacity. *PLoS Comput Biol.* **10**, e1003986 (2014).
- Chen, G., King, J. A., Lu, Y., Cacucci, F. & Burgess, N. Spatial cell firing during virtual navigation of open arenas by head-restrained mice. *Elife* **7**, e34789 (2018).
- Sheintuch, L. et al. Tracking the Same Neurons across Multiple Days in Ca2+ Imaging Data. *Cell Rep.* **21**, 1102–1115 (2017).
- Wirtshafter, H. S. & Disterhoft, J. F. In Vivo Multi-Day Calcium Imaging of CA1 Hippocampus in Freely Moving Rats Reveals a High Preponderance of Place Cells with Consistent Place Fields. *J. Neurosci.* **42**, 4538–4554 (2022).
- Blair, G. J. et al. Hippocampal place cell remapping occurs with memory storage of aversive experiences. *eLife* **12**, e80661 (2023).
- Zhou, Y.-Q. et al. Conjunctive vector coding and place coding in hippocampus share a common directional signal. 2023.06.02.543340 Preprint at <https://doi.org/10.1101/2023.06.02.543340> (2023).
- Geva, N., Deitch, D., Rubin, A. & Ziv, Y. Time and experience differentially affect distinct aspects of hippocampal representational drift. *Neuron* **111**, 2357–2366.e5 (2023).
- Khatib, D. et al. Active experience, not time, determines within-day representational drift in dorsal CA1. *Neuron* **111**, 2348–2356.e5 (2023).
- Malvache, A., Reichinnek, S., Villette, V., Haimerl, C. & Cossart, R. Awake hippocampal reactivations project onto orthogonal neuronal assemblies. *Science* **353**, 1280–1283 (2016).
- van de Ven, G. M., Trouche, S., McNamara, C. G., Allen, K. & Dupret, D. Hippocampal Offline Reactivation Consolidates Recently Formed Cell Assembly Patterns during Sharp Wave-Ripples. *Neuron* **92**, 968–974 (2016).
- Soltész, I. & Losonczy, A. CA1 pyramidal cell diversity enabling parallel information processing in the hippocampus. *Nat. Neurosci.* **21**, 484–493 (2018).

35. Cembrowski, M. S. & Spruston, N. Heterogeneity within classical cell types is the rule: lessons from hippocampal pyramidal neurons. *Nat. Rev. Neurosci.* **20**, 193–204 (2019).
36. Mizuseki, K., Diba, K., Pastalkova, E. & Buzsáki, G. Hippocampal CA1 pyramidal cells form functionally distinct sublayers. *Nat. Neurosci.* **14**, 1174–1181 (2011).
37. Danielson, N. B. et al. Sublayer-Specific Coding Dynamics during Spatial Navigation and Learning in Hippocampal Area CA1. *Neuron* **91**, 652–665 (2016).
38. Sharif, F., Tayebi, B., Buzsáki, G., Royer, S. & Fernandez-Ruiz, A. Subcircuits of Deep and Superficial CA1 Place Cells Support Efficient Spatial Coding across Heterogeneous Environments. *Neuron* **109**, 363–376.e6 (2021).
39. Thompson, L. T. & Best, P. J. Long-term stability of the place-field activity of single units recorded from the dorsal hippocampus of freely behaving rats. *Brain Res.* **509**, 299–308 (1990).
40. Kentros, C. et al. Abolition of long-term stability of new hippocampal place cell maps by NMDA receptor blockade. *Science* **280**, 2121–2126 (1998).
41. Hainmueller, T. & Bartos, M. Parallel emergence of stable and dynamic memory engrams in the hippocampus. *Nature* **558**, 292–296 (2018).
42. Rudy, J. W. & Morledge, P. Ontogeny of contextual fear conditioning in rats: Implications for consolidation, infantile amnesia, and hippocampal system function. *Behav. Neurosci.* **108**, 227–234 (1994).
43. Travaglia, A., Bisaz, R., Sweet, E. S., Blitzer, R. D. & Alberini, C. M. Infantile amnesia reflects a developmental critical period for hippocampal learning. *Nat. Neurosci.* **19**, 1225–1233 (2016).
44. Treves, A. & Rolls, E. T. Computational analysis of the role of the hippocampus in memory. *Hippocampus* **4**, 374–391 (1994).
45. Treves, A. & Rolls, E. T. What determines the capacity of auto-associative memories in the brain? *Netw.: Comput. Neural Syst.* **2**, 371–397 (1991).
46. Northoff, G. Sparse Coding and Neural Inhibition. in *Unlocking the Brain: Volume 1: Coding* (ed. Northoff, G.) 0 (Oxford University Press, 2013). <https://doi.org/10.1093/acprof:oso/9780199826988.003.0002>.
47. Donato, F., Jacobsen, R. I., Moser, M.-B. & Moser, E. I. Stellate cells drive maturation of the entorhinal-hippocampal circuit. *Science* **355**, eaai8178 (2017).
48. Ramsaran, A. I. et al. A shift in the mechanisms controlling hippocampal engram formation during brain maturation. *Science* **380**, 543–551 (2023).
49. Dumas, T. C. Late postnatal maturation of excitatory synaptic transmission permits adult-like expression of hippocampal-dependent behaviors. *Hippocampus* **15**, 562–578 (2005).
50. Blair, M. G. et al. Developmental Changes in Structural and Functional Properties of Hippocampal AMPARs Parallels the Emergence of Deliberative Spatial Navigation in Juvenile Rats. *J. Neurosci.* **33**, 12218–12228 (2013).
51. Kramár, E. A. & Lynch, G. Developmental and regional differences in the consolidation of long-term potentiation. *Neuroscience* **118**, 387–398 (2003).
52. Meredith, R. M., Floyer-Lea, A. M. & Paulsen, O. Maturation of Long-Term Potentiation Induction Rules in Rodent Hippocampus: Role of GABAergic Inhibition. *J. Neurosci.* **23**, 11142–11146 (2003).
53. Rigby, M. et al. Multi-synaptic boutons are a feature of CA1 hippocampal connections in the stratum oriens. *Cell Rep.* **42**, 112397 (2023).
54. Muessig, L., Hauser, J., Wills, T. J. & Cacucci, F. A Developmental Switch in Place Cell Accuracy Coincides with Grid Cell Maturation. *Neuron* **86**, 1167–1173 (2015).
55. Nadel, L. Some implications of postnatal hippocampal development. *Hippocampus* **32**, 98–107 (2022).
56. Carman, H. M. & Mactutus, C. F. Ontogeny of spatial navigation in rats: A role for response requirements? *Behav. Neurosci.* **115**, 870–879 (2001).
57. Palmer, L. & Lynch, G. A Kantian View of Space. *Science* **328**, 1487–1488 (2010).
58. Hensch, T. K. Critical period plasticity in local cortical circuits. *Nat. Rev. Neurosci.* **6**, 877 (2005).
59. Alberini, C. M. & Travaglia, A. Infantile Amnesia: A Critical Period of Learning to Learn and Remember. *J. Neurosci.* **37**, 5783–5795 (2017).
60. Keresztes, A., Ngo, C. T., Lindenberger, U., Werkle-Bergner, M. & Newcombe, N. S. Hippocampal Maturation Drives Memory from Generalization to Specificity. *Trends Cogn. Sci.* **22**, 676–686 (2018).
61. Cavalieri, D. et al. CA1 pyramidal cell diversity is rooted in the time of neurogenesis. *Elife* **10**, e69270 (2021).
62. Huszár, R., Zhang, Y., Blockus, H. & Buzsáki, G. Preconfigured dynamics in the hippocampus are guided by embryonic birthdate and rate of neurogenesis. *Nat. Neurosci.* **25**, 1201–1212 (2022).
63. Deguchi, Y., Donato, F., Galimberti, I., Cabuy, E. & Caroni, P. Temporally matched subpopulations of selectively interconnected principal neurons in the hippocampus. *Nat. Neurosci.* **14**, 495–504 (2011).
64. Cembrowski, M. S. et al. Spatial Gene-Expression Gradients Underlie Prominent Heterogeneity of CA1 Pyramidal Neurons. *Neuron* **89**, 351–368 (2016).
65. Harvey, R. E., Robinson, H. L., Liu, C., Oliva, A. & Fernandez-Ruiz, A. Hippocampo-cortical circuits for selective memory encoding, routing, and replay. *Neuron* **111**, 2076–2090.e9 (2023).
66. Cheng, S. et al. Vision-dependent specification of cell types and function in the developing cortex. *Cell* **185**, 311–327.e24 (2022).
67. Mizuseki, K. & Buzsáki, G. Preconfigured, skewed distribution of firing rates in the hippocampus and entorhinal cortex. *Cell Rep.* **4**, 1010–1021 (2013).
68. Rich, P. D., Liaw, H.-P. & Lee, A. K. Large environments reveal the statistical structure governing hippocampal representations. *Science* **345**, 814–817 (2014).
69. Lee, D., Lin, B.-J. & Lee, A. K. Hippocampal Place Fields Emerge upon Single-Cell Manipulation of Excitability During Behavior. *Science* **337**, 849–853 (2012).
70. Lee, J. S., Briguglio, J. J., Cohen, J. D., Romani, S. & Lee, A. K. The Statistical Structure of the Hippocampal Code for Space as a Function of Time, Context, and Value. *Cell* **183**, 620–635.e22 (2020).
71. Buzsáki, G. Our skewed sense of space. *Science* **347**, 612–613 (2015).
72. Grosmark, A. D. & Buzsáki, G. Diversity in neural firing dynamics supports both rigid and learned hippocampal sequences. *Science* **351**, 1440–1443 (2016).
73. McKenzie, S. et al. Preexisting hippocampal network dynamics constrain optogenetically induced place fields. *Neuron* **109**, 1040–1054.e7 (2021).
74. Aronov, D. & Tank, D. W. Engagement of neural circuits underlying 2D spatial navigation in a rodent virtual reality system. *Neuron* **84**, 442–456 (2014).
75. Pnevmatikakis, E. A. & Giovannucci, A. NoRMCorre: An online algorithm for piecewise rigid motion correction of calcium imaging data. *J. Neurosci. Methods* **291**, 83–94 (2017).
76. Zhou, P. et al. Efficient and accurate extraction of in vivo calcium signals from microendoscopic video data. *Elife* **7**, e28728 (2018).
77. Pachitariu, M. et al. Suite2p: beyond 10,000 neurons with standard two-photon microscopy. 061507 Preprint at <https://doi.org/10.1101/061507> (2017).
78. Chen, T.-W. et al. Ultrasensitive fluorescent proteins for imaging neuronal activity. *Nature* **499**, 295–300 (2013).

79. Scholl, B., Thomas, C. I., Ryan, M. A., Kamasawa, N. & Fitzpatrick, D. Cortical response selectivity derives from strength in numbers of synapses. *Nature* **590**, 111–114 (2021).
80. Vogelstein, J. T. et al. Fast Nonnegative Deconvolution for Spike Train Inference From Population Calcium Imaging. *J. Neurophysiol.* **104**, 3691–3704 (2010).
81. Mathis, A. et al. DeepLabCut: markerless pose estimation of user-defined body parts with deep learning. *Nat. Neurosci.* **21**, 1281–1289 (2018).
82. Skaggs, W. E., McNaughton, B. L., Gothard, K. M. & Markus, E. J. An information-theoretic approach to deciphering the hippocampal code. in *Proceedings of the 5th International Conference on Neural Information Processing Systems* 1030–1037 (Morgan Kaufmann Publishers Inc., San Francisco, CA, USA, 1992).
83. Kaufman, L. & Rousseeuw, P. J. Finding Groups in Data: An Introduction to Cluster Analysis. (1990).
84. Romano, S. A. et al. An integrated calcium imaging processing toolbox for the analysis of neuronal population dynamics. *PLOS Comput. Biol.* **13**, e1005526 (2017).
85. Heeger, D. Poisson Model of Spike Generation. (2000).
86. Wang, C.-Y. et al. Early and late place cells during postnatal development of the hippocampus. *Zenodo*, <https://doi.org/10.5281/zenodo.13911919> (2024).

Acknowledgements

We thank the PKU-Nanjing Joint Institute of Translational Medicine (Nanjing 211800, China) for assistance in data acquisition with the miniature two-photon microscope. We thank Li Wang for the technical help in the virtual reality setup. This study was supported by the following grants: STI2030-Major Projects (2022ZD0205500) to X.C., Guangdong Basic and Applied Basic Research Foundation (2022A1515010799) to X.C., Shenzhen Key Laboratory of Precision Diagnosis and Treatment of Depression (ZDSYS20220606100606014) to C.W., National Natural Science Foundation of China (32171043) to C.W., CAS Key Laboratory of Brain Connectome and Manipulation (2019DP173024) to C.W., Guangdong Provincial Key Laboratory of Brain Connectome and Behavior (2023B1212060055) to C.W.

Author contributions

X.C. and C.W. conceived and supervised the study; C.-Y.W. and S.C. performed recording experiments; H.Y. and C.-Y.W. performed data

analyses; X.C., C.W., C.-Y.W., and H.Y. wrote the manuscript. All authors commented on the manuscript.

Competing interests

The authors declare no competing interests.

Additional information

Supplementary information The online version contains supplementary material available at <https://doi.org/10.1038/s41467-024-54320-z>.

Correspondence and requests for materials should be addressed to Cheng Wang or Xiaojing Chen.

Peer review information *Nature Communications* thanks Paul Frankland and the other, anonymous, reviewer(s) for their contribution to the peer review of this work. A peer review file is available.

Reprints and permissions information is available at <http://www.nature.com/reprints>

Publisher's note Springer Nature remains neutral with regard to jurisdictional claims in published maps and institutional affiliations.

Open Access This article is licensed under a Creative Commons Attribution-NonCommercial-NoDerivatives 4.0 International License, which permits any non-commercial use, sharing, distribution and reproduction in any medium or format, as long as you give appropriate credit to the original author(s) and the source, provide a link to the Creative Commons licence, and indicate if you modified the licensed material. You do not have permission under this licence to share adapted material derived from this article or parts of it. The images or other third party material in this article are included in the article's Creative Commons licence, unless indicated otherwise in a credit line to the material. If material is not included in the article's Creative Commons licence and your intended use is not permitted by statutory regulation or exceeds the permitted use, you will need to obtain permission directly from the copyright holder. To view a copy of this licence, visit <http://creativecommons.org/licenses/by-nc-nd/4.0/>.

© The Author(s) 2024